UNIVERSITY OF WEST LONDON
The Career University

UWL REPOSITORY

repository.uwl.ac.uk

Soil texture influences the magnitude and depth persistence of alfalfa reinforcement and its contribution to slope stability

Rahim, Amara and Naveed, Muhammad ORCID logoORCID: https://orcid.org/0000-0002-0923-4976 (2026) Soil texture influences the magnitude and depth persistence of alfalfa reinforcement and its contribution to slope stability. Geotechnics, 6 (4).

https://doi.org/10.3390/geotechnics6040118

This is the Published Version of the final output.

UWL repository link: https://repository.uwl.ac.uk/id/eprint/15782/

Alternative formats: If you require this document in an alternative format, please contact: open.research@uwl.ac.uk

Copyright: Creative Commons: Attribution 4.0

Copyright and moral rights for the publications made accessible in the public portal are retained by the authors and/or other copyright owners and it is a condition of accessing publications that users recognise and abide by the legal requirements associated with these rights.

Take down policy: If you believe that this document breaches copyright, please contact us at open.research@uwl.ac.uk providing details, and we will remove access to the work immediately and investigate your claim.

Rights Retention Statement:

geotechnics

MDPI

Article

Soil Texture Influences the Magnitude and Depth Persistence of Alfalfa Reinforcement and Its Contribution to Slope Stability

Amara Rahim and Muhammad Naveed *

School of Computing and Engineering, University of West London, St Mary's Road, Ealing, London W5 5RF, UK
* Correspondence: muhammad.naveed@uwl.ac.uk

Abstract

Vegetation-based slope stabilisation depends on coupled mechanical and hydraulic processes that vary with soil texture and depth. This study linked a five-month long, 0.5 m column experiment to annual two-dimensional transient seepage and analytical infinite-slope modelling to quantify how alfalfa (*Medicago sativa* L.) and a mycorrhiza-containing formulation affect shallow root-zone stability in silty clay (SC) and silty sand (SS). Eighteen columns (n = 3 per soil–treatment combination) received unplanted control (C), alfalfa (A), or alfalfa plus mycorrhiza formulation (A + MF). Biomass, saturated hydraulic conductivity (k_s), and saturated direct-shear response at six depths were measured. Relative to A, A + MF increased recovered root dry mass by 24.5% in SC and 53.2% in SS, and k_s by 46.6% and 47.4%. Factorial ANOVA detected a soil × treatment interaction for k_s ($p = 0.00052$), but not biomass. Exponential apparent-cohesion profiles separated reinforcement amplitude from depth persistence; fitted decay depths for A/A + MF were 0.167/0.176 m in SC and 0.064/0.22 m in SS. The measured mechanical and hydraulic parameters were applied to a 365-day model of a representative 1V:3H natural infinite slope. All planted cases retained higher annual minimum root-zone factors of safety than their controls, but retention, uptake and storm-timing sensitivities changed the A versus A + MF ranking. Reinforcement magnitude, depth persistence, and soil-specific hydrology should therefore be represented together when evaluating biologically treated shallow slopes.

Keywords: soil bioengineering; Medicago sativa; mycorrhiza-containing formulation; root reinforcement; apparent cohesion; unsaturated seepage; infinite slope; shallow slope stability

Check for updates

Academic Editors: Geetanjali Das, Snehasis Tripathy and Ankit Garg

Received: 16 September 2026
Revised: 18 October 2026
Accepted: 28 October 2026
Published: 4 November 2026

Copyright: © 2026 by the authors. Licensee MDPI, Basel, Switzerland. This article is an open access article distributed under the terms and conditions of the Creative Commons Attribution (CC BY) license.

1. Introduction

Alternating intense rainfall and drying can destabilise natural slopes, transportation earthworks and embankments through rapid loss of matric suction, pore-pressure rise, surface erosion and desiccation-related deterioration [1,2]. Conventional structural measures remain essential where large stabilising forces are required, but soil bioengineering is increasingly used as a complementary nature-based strategy because it can combine erosion control, shallow mechanical reinforcement and hydrological regulation with ecological co-benefits [3–5].

Vegetation modifies slope behaviour through coupled mechanical and hydraulic mechanisms. Mechanical reinforcement develops through root tensile resistance, root–soil interface friction, branching and anchorage, and the spatial distribution of roots relative to potential shear surfaces [6–9]. Hydraulic effects include interception, root water uptake, evapotranspiration-induced suction, and biologically induced changes in pore structure,

water retention and hydraulic conductivity [10–14]. These processes need not act in the same direction: root water uptake can promote inter-event drying, while root-generated macropores and increases in saturated conductivity can accelerate water redistribution during wetting [15,16].

The relative contribution of hydraulic and mechanical reinforcement is time-dependent. Hydrological reinforcement can be substantial during drying but may diminish during prolonged rainfall as suction collapses, whereas mechanical root reinforcement can remain mobilisable after wetting [11,12]. Biomass, k_s or a dry-condition strength increment is therefore insufficient as a standalone indicator of slope performance. The broader soil–vegetation–atmosphere (SVA) framework describes exchanges of water and energy at the ground surface as a coupled thermo–hydro–mechanical boundary condition, with processes operating from root and pore scales to the slope scale [17,18]. This perspective motivates combining depth-dependent mechanical reinforcement, hydraulic properties and atmospheric forcing. The present framework represents hydraulic forcing and its effect on shear resistance; heat transport, temperature-dependent constitutive behaviour and deformation feedback to seepage were not modelled.

In engineering models, root reinforcement is frequently represented as additional or apparent cohesion, c_a [19]. Such a representation is convenient but can become misleading if a single value is assigned through an entire nominal root zone. Root abundance and mobilisation generally decrease with depth, and field-scale stability is sensitive to the spatial distribution of root cohesion [9,20]. Root-bundle approaches similarly show that reinforcement is governed by the progressive mobilisation and failure of distributed roots rather than a spatially uniform increment [21]. A depth-resolved formulation can therefore retain two distinct engineering attributes: the magnitude of reinforcement near the surface and the depth over which that reinforcement persists.

Alfalfa (*Medicago sativa* L.) is a perennial tap-rooted legume with a dominant root axis and finer lateral roots. Previous experiments have demonstrated increases in soil shear resistance associated with alfalfa roots, although the response varies with root development, soil texture, stress level and water condition [22,23]. More broadly, root-system shear behaviour varies with root architecture and land-use conditions [24]. The rhizosphere may be further altered by microbial associations. Arbuscular mycorrhizal fungi can affect nutrient acquisition, plant–water relations and aggregation [25,26], and direct evidence demonstrates fungal pathways for water transport to host plants [27]. Mycorrhizal effects on water retention and hydraulic conductivity can also be texture-dependent [13], while inoculation has been associated with improved root development and aggregate stability in eco-engineering contexts [28,29].

At the same time, biological attribution requires care. Commercial inoculants may contain multiple microorganisms and biostimulant constituents, and demonstration of a specifically mycorrhizal mechanism requires colonisation measurements or appropriately controlled inoculation experiments. Accordingly, the present study treats A + MF versus A as the incremental response to a commercial mycorrhiza-containing formulation rather than proof of fungal causation or plant–fungus synergy. This distinction is consistent with the stronger causal evidence available from studies that explicitly trace fungal persistence or quantify colonisation [30,31].

The study links depth-resolved saturated mechanical measurements and treatment-specific saturated conductivity to annual root-zone slope stability. The objectives were to: (i) compare alfalfa biomass and k_s and test soil × treatment interactions in two soils; (ii) characterise mobilised saturated shear resistance at six depths to 0.5 m; (iii) describe reinforcement magnitude and depth persistence; and (iv) examine the measured parameter sets in a transient seepage model coupled to an infinite-slope calculation with a time-

dependent critical depth. We hypothesised that A + MF would increase below-ground development and mechanical reinforcement relative to A, while the observed magnitude, persistence and simulated stability response would differ between the two soils.

2. Materials and Methods

2.1. Soils and Biological Treatments

Both soils were sampled from Maidenhead, Berkshire, United Kingdom. They were dried at 40 °C for 48 h, gently disaggregated and passed through a 2 mm sieve. Sample preparation, particle-size analysis and consistency-limit testing followed BS 1377-1:2016 and BS 1377-2:2022 [32,33]. Particle-size distributions were determined by wet sieving and hydrometer analysis; liquid and plastic limits were determined by cone penetration and thread rolling. The fine-grained soil contained 36% clay, 32% silt and 32% sand, with liquid limit 31%, plastic limit 22% and plasticity index 9%. The coarser soil contained 21% clay, 19% silt and 60% sand, with corresponding limits of 26%, 24% and 2%. The descriptive labels silty clay (SC) and silty sand (SS) are used throughout. Standard Proctor tests followed BS 1377-4:1990 [34]; maximum dry unit weights were 16.4 and 17.1 kN m^{-3} and optimum moisture contents were 18% and 16% for SC and SS, respectively (Figure 1).

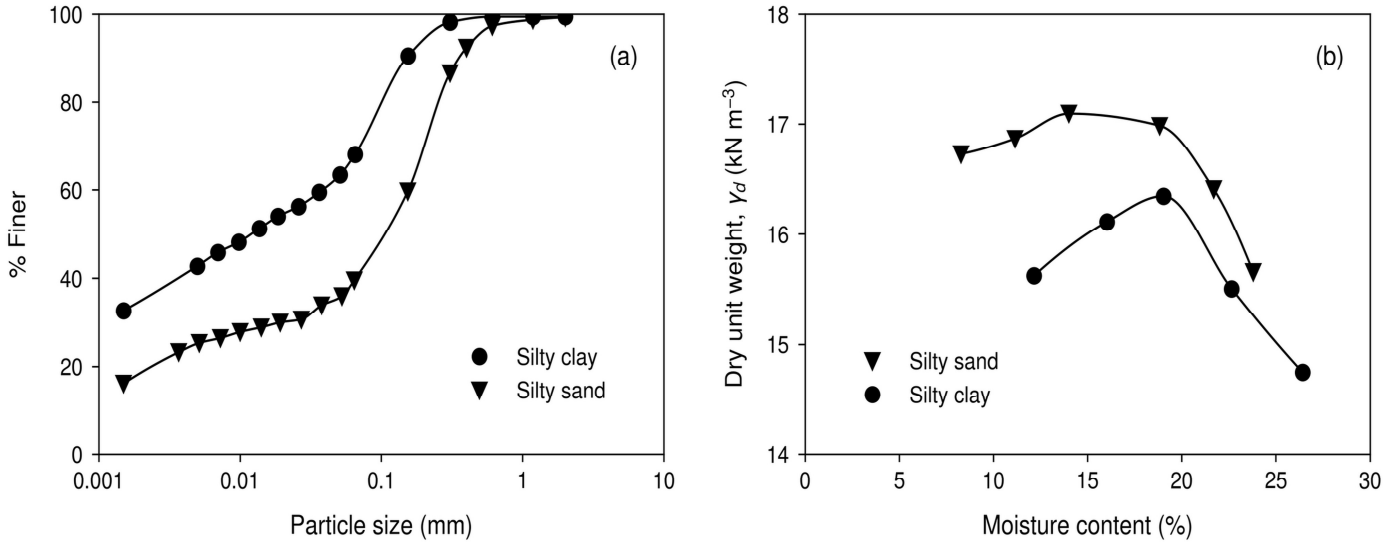


Figure 1. Physical characterisation of the study soils: (**a**) particle-size distributions and (**b**) standard Proctor dry unit weight versus moisture content. SC and SS denote silty clay and silty sand in the manuscript.

Alfalfa (*Medicago sativa* L.; Fabaceae) seed was obtained from Pretty Wild Seeds and soaked in water for 48 h before sowing. TNC MycorrMax (The Nutrient Company, Littleborough, UK) was used for the microbial treatment. Product information describes a multi-component formulation containing endomycorrhizal and ectomycorrhizal fungi, *Trichoderma* and *Bacillus* species, and humic and seaweed-derived constituents. Root colonisation, inoculant establishment and the contributions of individual constituents were not quantified; the treatment is therefore termed a mycorrhiza-containing formulation (MF), and A + MF denotes a formulation-level treatment rather than a verified fungal symbiosis.

2.2. Column Preparation and Growth Conditions

The experimental design comprised two soils and three treatments, with three independent columns per combination (18 columns in total; Figure 2). The final column configuration was 500 mm high and 100 mm in internal diameter (Figure 3). Nylon-mesh bases permitted drainage. Soil was compacted in successive layers to 80% of its maximum

dry unit weight, with each layer surface scarified before placement of the next. Preparation moisture contents were 18% for SC and 16% for SS. These values describe specimen preparation and are distinguished from the slope-model unit weights in Section 2.5.1.

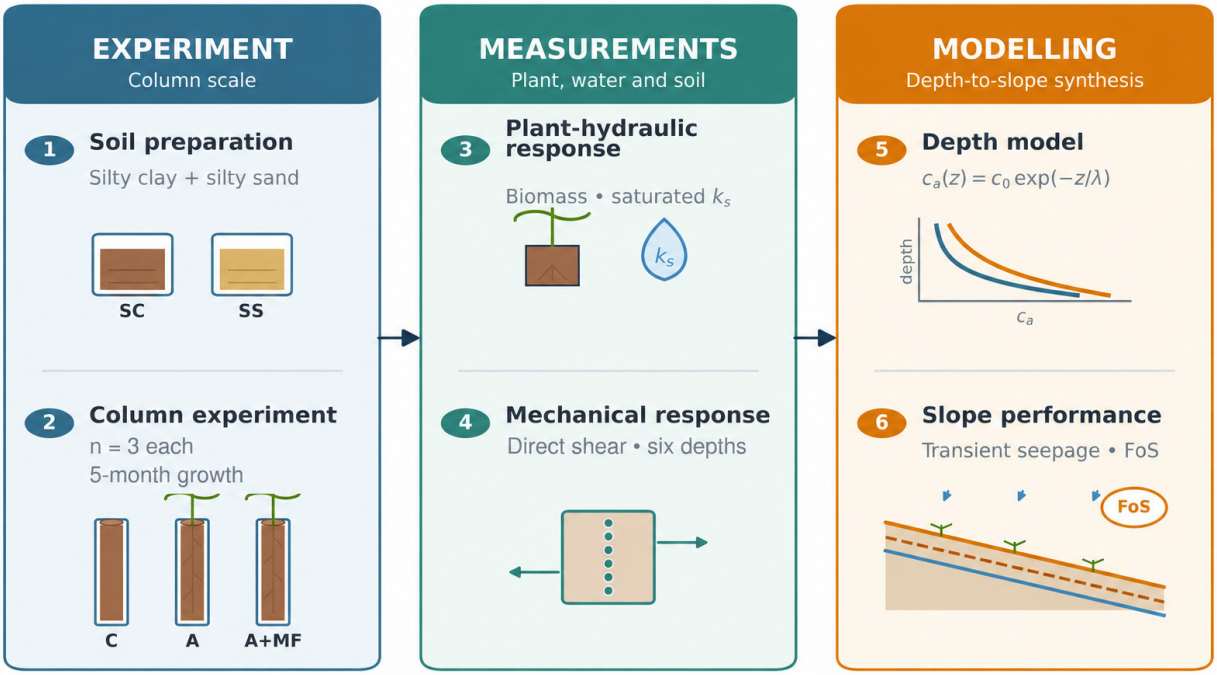


Figure 2. Workflow linking the five-month column experiment, biomass and hydraulic measurements, direct-shear characterisation at six depths, exponential apparent-cohesion profiles and transient root-zone stability. C, unplanted control; A, alfalfa; A + MF, alfalfa with the commercial mycorrhiza-containing formulation. Soil abbreviations in the text are SC and SS for silty clay and silty sand, respectively.

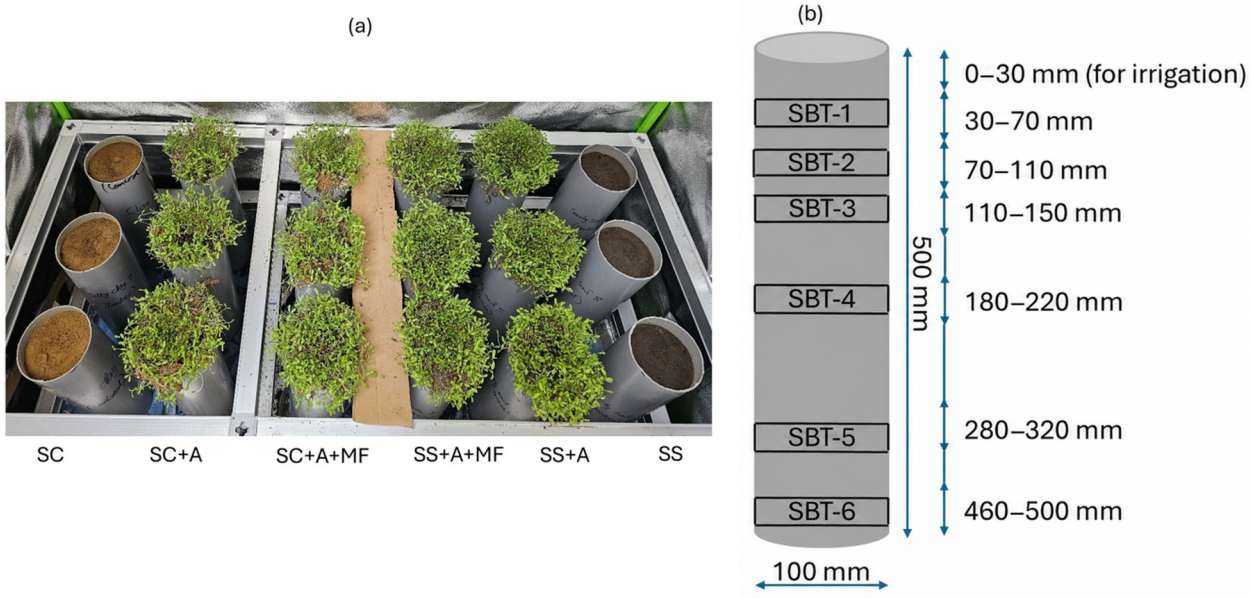


Figure 3. Experimental arrangement and sampling: (**a**) greenhouse columns for the two soils and three treatments; (**b**) final column dimensions and six extraction intervals (SBT–1 to SBT–6), represented by depths of 0.05, 0.09, 0.13, 0.20, 0.30 and 0.48 m. SC, silty clay; SS, silty sand; A, alfalfa; MF, commercial mycorrhiza-containing formulation.

Each A column received 5 g of pre-soaked seed. For A + MF, 16.5 g of inoculant was mixed with the soil before compaction and sowing. Controls contained neither seed nor inoculant. Columns were maintained in a naturally ventilated greenhouse for five months, with lighting conditions described below. Each initially received 200 mL of water and subsequently 50 mL twice weekly. Once weekly, planted columns additionally received 100 mL of diluted low-phosphorus Growth Technology Formulex nutrient solution; controls received 100 mL of water. Planted-versus-control comparisons therefore include a nutrient-management difference. The A + MF-versus-A comparison shares the planting, irrigation and nutrient regime and more closely isolates the incremental formulation response.

The plant columns were cultivated for five months (April–September 2025) in an indoor greenhouse equipped with LED grow lights. The LED lights were operated for 10 h daily using an automatic timer, while additional natural daylight entered through the transparent greenhouse enclosure. Consequently, the total photoperiod varied with seasonal daylight conditions. Photosynthetically active radiation (PAR) and light intensity were not measured. Greenhouse temperature and relative humidity were monitored three times weekly, ranging from 17.2 to 27.3 °C and 31% to 64%, respectively. Soil pH, measured during direct-shear specimen preparation, was 6.8 for both soils across all treatments.

2.3. Experimental Measurements

2.3.1. Plant Growth and Biomass

Seedling emergence was observed within two days and shoot height was measured weekly. At harvest, shoots were cleaned and dried at 60 °C for 72 h. Roots were recovered by gently washing soil through a 1 mm sieve, hand-picked with tweezers and dried at 60 °C for 48 h. Dry masses were determined separately for shoots and roots. Recovered root mass represents the fraction retained by this procedure; very fine roots and hyphae were not quantified independently.

2.3.2. Soil Water Retention

Drying soil-water-retention curves (SWRCs) were determined in triplicate for each soil using contact filter paper. The specimens, 50 mm in diameter and 50 mm high, were prepared in steel rings at 80% of the respective maximum dry density, saturated and progressively dried. At each water-content stage, Whatman No. 42 filter paper from a common batch was placed against the soil and sealed in an airtight container for at least seven days at stable laboratory temperature. Papers were handled using clean, dry tweezers, weighed promptly to 0.0001 g, dried at 105 ± 2 °C for at least 24 h and reweighed after cooling in a desiccator.

Matric suction ψ (kPa) was obtained from filter-paper gravimetric water content, w (%), using the Chandler et al. [35] calibration: $\log_{10}\psi = 4.84 - 0.0622\ w$ for $w < 47\%$, and $\log_{10}\psi = 6.05 - 2.48\log_{10} w$ for $w \geq 47\%$. The soil water content at each stage was calculated from the moist mass and final oven-dry mass and converted to volumetric water content using dry density. Retention parameters were fitted separately for SC and SS and assigned identically to C, A and A + MF within each soil. This was a modelling assumption, not evidence that the root–soil composites had identical retention. Treatment-specific retention curves and wetting–drying hysteresis were not characterised.

2.3.3. Saturated Hydraulic Conductivity

Saturated hydraulic conductivity, k_s, was measured on intact columns by the falling-head method following BS 1377-5:1990 [36]. Columns were saturated before testing. Conductivity was calculated as:

$$k_s = \frac{aL}{A\Delta t}\ln\left(\frac{h_1}{h_2}\right) \quad (1)$$

where a and A are the standpipe and specimen cross-sectional areas, L is the tested soil length, Δt is elapsed time, and h_1 and h_2 are the initial and final head differences. Consistent length and time units were used before conversion to m d^{-1}. The three columns in each soil–treatment combination provided the independent conductivity measurements.

2.3.4. Saturated Direct-Shear Tests

Specimens measuring 60 × 60 × 20 mm were recovered from six depth intervals: 30–70, 70–110, 110–150, 180–220, 280–320 and 460–500 mm. Their representative depths were 0.05, 0.09, 0.13, 0.20, 0.30 and 0.48 m (Figure 3). The sampling intervals identify the extraction bands, whereas 20 mm is the thickness of the trimmed shear specimen. Testing used a digital ELE direct-shear apparatus with calibrated load and displacement transducers. Specimens were saturated for 24 h, consolidated under the target normal stress and sheared under drained conditions at 0.025 mm min^{-1} to 7.5 mm horizontal displacement; observations were recorded every 0.1 mm.

Within each soil–treatment combination, one column was assigned to each normal stress of 37, 69 and 100 kPa. Each depth-specific envelope therefore used three specimens from different columns, with no replication at a given normal stress. Specimens at different depths from the same column were not independent column replicates. Horizontal displacement at termination was δh = 7.5 mm. The dimensionless displacement ratio $\delta h/L_0$ was 0.125, or 12.5%, where L_0 = 60 mm is the initial specimen length. This index is termed normalised horizontal displacement. No distinct peak was reached, so terminal shear stress at $\delta h/L_0$ = 12.5%, denoted $\tau_{12.5}$, defined the common mobilised envelope.

2.3.5. Statistical Analysis

Each response was analysed using a fixed-effects two-way ANOVA including soil, treatment and their interaction. The conductivity model comprised two soils (SC and SS) × three treatments (C, A and A + MF), with three independent columns per combination (18 observations; 12 residual degrees of freedom). Separate shoot- and root-mass models comprised two soils × two planted treatments (A and A + MF), with three columns per combination (12 observations; eight residual degrees of freedom); unplanted controls were not entered as zero biomass observations. Original-scale analyses tested absolute differences in the measured responses. A separate ANOVA of $\ln(k_s)$ assessed whether the conductivity interaction also held for proportional responses. Residual normality and variance homogeneity were examined using Shapiro–Wilk and median-centred Levene tests. All pairwise soil–treatment means were compared using Tukey's honestly significant difference test with the factorial model's pooled residual variance: one family of 6 comparisons among four means for each biomass response, and one family of 15 comparisons among six conductivity means. Tukey-adjusted p-values and simultaneous 95% confidence intervals were calculated; significance was assessed at $p < 0.05$. The root-to-shoot index remained the ratio of treatment mean root and shoot dry masses and was not tested inferentially.

2.4. Data Reduction and Depth-Resolved Reinforcement

Biomass and k_s are reported as means and standard errors from three independent columns per soil–treatment combination. Percentage differences between A + MF and A were calculated as 100[(A + MF)/A − 1] and treated as descriptive effect sizes. Strength parameters were obtained from depth-specific mobilised envelopes of the following form:

$$\tau_{12.5} = c_a + \sigma_n \tan\phi_m \quad (2)$$

where c_a is the apparent cohesion, σ_n is applied normal stress and ϕ_m is the mobilised friction angle. The apparent-cohesion term represents the treatment-associated response of

the root–soil composite, including possible structural and stress-range effects. The depth dependence of apparent cohesion was represented by

$$c_a(z) = c_0\, e^{-z/\lambda c} \quad (3)$$

where c_0 is the extrapolated apparent cohesion at the ground surface (kPa) and λ_c is the characteristic decay depth (m), at which c_a falls to c_0/e. Exponential profiles were fitted by ordinary least squares on $\ln(c_a)$ using the positive values in Table 1, retaining their numerical precision during fitting. The zero SS–A value at 0.48 m was excluded because its logarithm is undefined. The profile is defined over 0–0.50 m, with c_a set to zero below that depth. The integrated apparent-cohesion index was:

$$I_c = \int_0^{z_r} c_a(z)\, dz = c_0\lambda_c\left[1 - \exp\left(\frac{-z_r}{\lambda_c}\right)\right] \quad (4)$$

with z_r = 0.50 m. I_c has units of kPa·m and is the area under the apparent-cohesion–depth profile. It combines amplitude and persistence for comparisons over the same integration depth. It is neither a local cohesion nor a resisting force and was not assigned directly to a candidate slip plane.

Table 1. Depth-specific apparent cohesion (c_a) and mobilised friction angle (ϕ_m) used to parameterise the root zone.

Depth (m)	Quantity	SC-C	SC-A	SC-A + MF	SS-C	SS-A	SS-A + MF
0.05	c_a (kPa)	0	3.765	4.710	0	0.750	1.545
	ϕ_m (°)	19.0	22.0	23.0	25.0	26.0	27.0
0.09	c_a (kPa)	0	3.165	3.495	0	0.450	1.350
	ϕ_m (°)	19.0	22.0	23.0	25.0	26.0	27.0
0.13	c_a (kPa)	0	2.175	2.850	0	0.150	1.050
	ϕ_m (°)	19.0	22.0	23.0	25.0	26.5	27.5
0.20	c_a (kPa)	0	1.500	1.800	0	0.075	0.750
	ϕ_m (°)	19.5	22.5	23.5	25.5	27.0	28.0
0.30	c_a (kPa)	0	0.750	1.050	0	0.015	0.450
	ϕ_m (°)	19.5	22.5	23.5	25.5	27.0	28.0
0.48	c_a (kPa)	0	0.300	0.400	0	0.000	0.225
	ϕ_m (°)	19.5	22.5	23.5	25.5	27.0	28.0

SC, silty clay; SS, silty sand; A, alfalfa; A + MF, alfalfa with the mycorrhiza-containing formulation. Positive c_a values define the exponential fits in Table 2.

Table 2. Exponential apparent-cohesion profiles and integrated reinforcement over 0–0.50 m.

Soil	Treatment	c_0 (kPa)	λ_c (m)	I_c (kPa·m)
Silty clay	A	5.002	0.1669	0.793
	A + MF	5.926	0.1759	0.981
Silty sand	A	1.556	0.0643	0.100
	A + MF	1.927	0.2182	0.378

2.5. Transient Seepage and Root-Zone Stability

2.5.1. Numerical Framework and Slope Representation

A sequential seepage–stability framework was implemented in Python 3.12. Transient unsaturated seepage was solved in a two-dimensional slope-aligned domain per unit out-of-plane width and passed to an analytical infinite-slope calculation. Coupling was one-way: deformation did not modify hydraulic properties or flow. The six baseline cases combined measured treatment-specific conductivity and strength profiles for C, A and A + MF in each soil. Additional matched-input cases separated the effects of replacing the mechanical profile from those of replacing the hydraulic treatment inputs.

The slope was idealised as a translationally invariant natural slope with a gradient of 1V:3H ($\beta = 18.435°$), without an assigned crest, toe or bench (Figure 4). The local hydraulic window was 6.0 m horizontally, equivalent to 6.325 m along the slope, and 4.0 m in vertical depth. The vertical depth below ground is z. The treatment and uptake zone extended to 0.50 m; the lower boundary was treated as a no-flow soil–bedrock boundary. Apparent cohesion and root uptake were set to zero below 0.50 m, while host–soil friction remained available. Constant nominal bulk unit weights of 15.48 kN m^{-3} for SC and 15.87 kN m^{-3} for SS were assigned to the slope stability calculations across all treatments. These values were calculated as $\gamma = 0.8\gamma_{d,max}(1 + w_{OMC})$, representing a reference condition at 80% MDD and OMC.

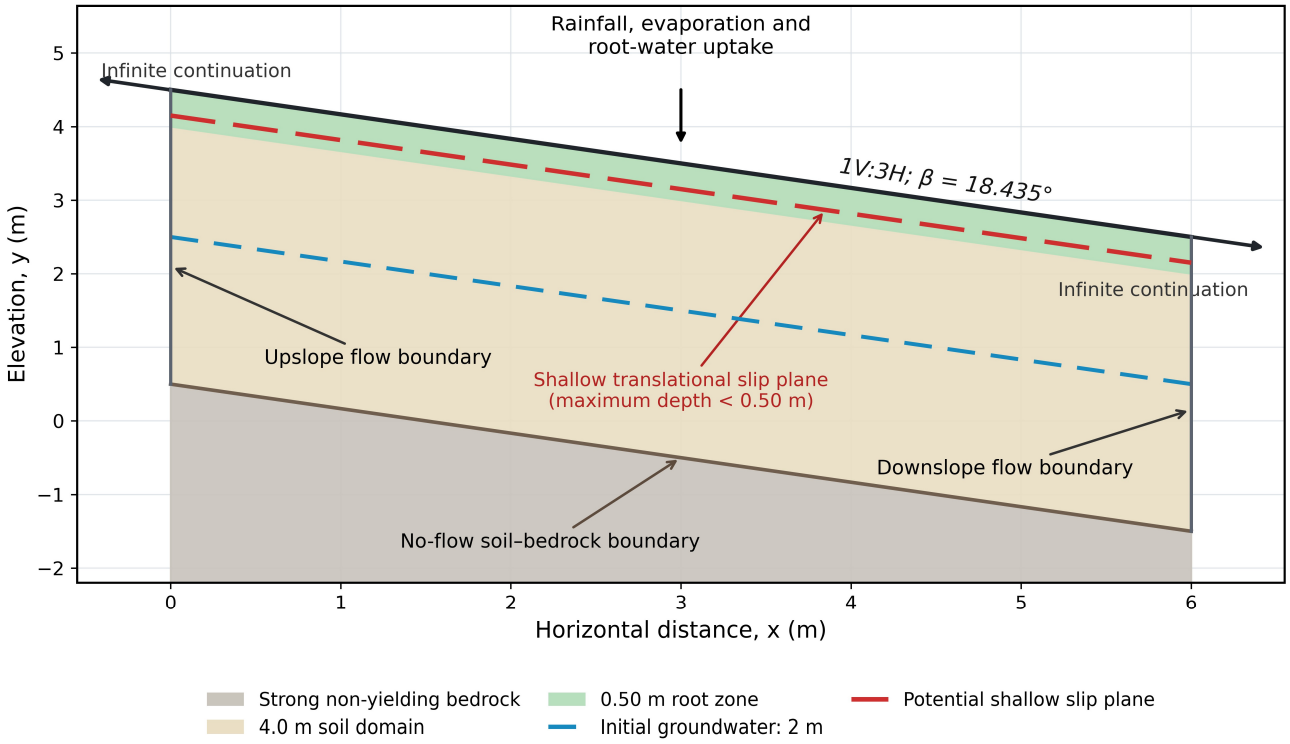


Figure 4. Local hydraulic window for the natural infinite-slope idealisation. Ground, root-zone boundary, candidate translational plane and lower continuation plane are parallel. Both lateral faces connect to the same-soil continuation through flow boundaries; the lower face has zero normal Darcy flux. The dashed initial groundwater line is 2 m vertically below ground and is not a fixed-head boundary. No finite crest or toe geometry is assigned.

The finite window is a local computational segment of an infinitely continuing, uniform natural slope rather than a finite embankment cross-section. Its lateral faces truncate the upslope and downslope continuations and were treated as flow boundaries. The mechanical idealisation comprised planar translational slip surfaces parallel to the ground

surface, so only the candidate vertical depth varied; circular and compound surfaces were outside the model definition.

2.5.2. Transient Seepage, Climate Forcing and Hydraulic Boundaries

Transient water flow was described by the mixed-form Richards equation [37]:

$$\frac{\partial \theta(h)}{\partial t} = \nabla \cdot [k(h)\nabla(h + z_e)] - S_r, \tag{5}$$

where θ is volumetric water content, h is pressure head, z_e is elevation head, k is hydraulic conductivity and S_r is root water extraction. Soil water retention and unsaturated conductivity followed the van Genuchten [38] and Mualem [39] relationships:

$$S_e(h) = \begin{cases} \left[1 + (\alpha|h|)^n\right]^{-m}, & h < 0, \\ 1, & h \geq 0, \end{cases} \qquad \theta(h) = \theta_r + (\theta_s - \theta_r)S_e(h) + S_s \max(h, 0), \tag{6}$$

$$K(h) = K_s S_e^l \left[1 - \left(1 - S_e^{1/m}\right)^m\right]^2, \qquad m = 1 - \frac{1}{n} \tag{7}$$

Here, S_e is effective saturation, $S_s = 1.0 \times 10^{-4}$ m^{-1} is specific storage, and the remaining parameters have their conventional meanings. Retention parameters were common among treatments within each soil, whereas measured saturated hydraulic conductivity, k_s, was treatment-specific (Table 3). Hydraulic anisotropy, hysteresis, treatment-dependent retention curves, and seasonal changes in hydraulic properties were not represented.

Table 3. Hydraulic parameters used in the transient seepage analysis.

Parameter	Silty Clay	Silty Sand
Residual water content, θ_r (m^3 m^{-3})	0.0882	0.0656
Saturated water content, θ_s (m^3 m^{-3})	0.4679	0.4329
van Genuchten α (m^{-1})	1.3257	2.0406
van Genuchten n	1.4198	1.4330
$m = 1 - \frac{1}{n}$	0.2957	0.3022
Pore-connectivity parameter, l	0.5	0.5
k_s, C (m d^{-1})	0.066	0.198
k_s, A (m d^{-1})	0.188	0.417
k_s, A + MF (m d^{-1})	0.277	0.616

Equation (5) was solved on a grid comprising eight cells along the slope and 96 layers perpendicular to the slope surface, giving 768 calculation cells. Backward-Euler time integration was used, and hydraulic conductivity at each cell interface was calculated using the harmonic mean of the neighbouring cell values. At each time step, Newton iteration solved the discrete water-balance equations. The final implementation used a direct sparse Newton solver that incorporated switching between atmospheric flux and pressure boundary conditions within these equations. Modified Picard iteration and time-step halving were available as fallback methods when convergence was difficult. Newton convergence required the sum of the absolute cell water-volume residuals to be $\leq 10^{-6}$ m^2 per unit width; this tolerance was tightened to 10^{-8} m^2 in the final direct solver. The standard Picard settings were a pressure-head change tolerance of 10^{-6} m and a maximum of 200 iterations. During difficult transitions, stronger under-relaxation and up to 1000 iterations were permitted, with the head-change tolerance relaxed to no more than 10^{-3} m, provided that the summed absolute water-volume residual remained $\leq 10^{-5}$ m^2 per unit width. Results were recorded every 6 h. The 365–day simulation covered 16 July 2020–

15 July 2021, using Whiteknights rainfall [40] and gridded Penman–Monteith reference potential evapotranspiration (PET) [41,42], with annual totals of 784.3 and 612.72 mm, respectively (Figure 5). In the baseline simulation, daily rainfall and PET totals were distributed uniformly over 24 h. Separate hourly event replays examined the effects of rainfall timing.

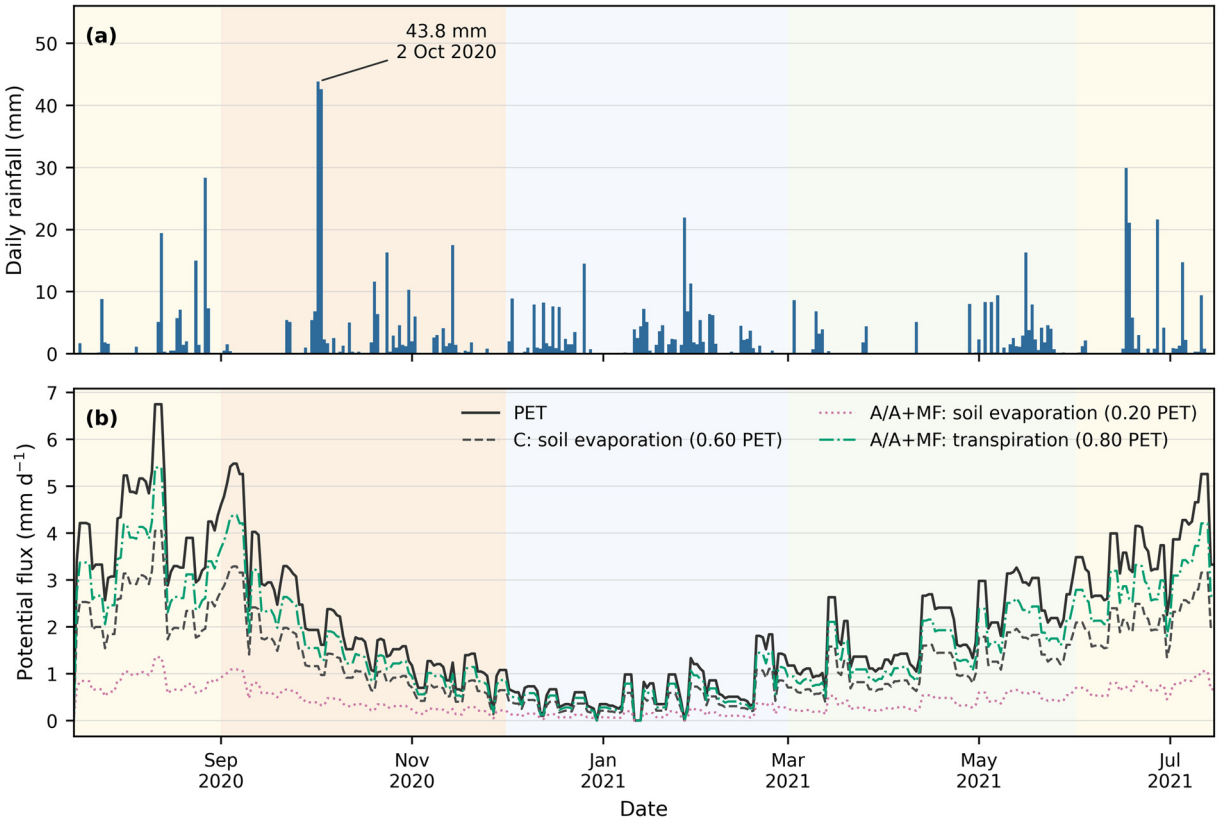


Figure 5. Daily rainfall and potential water fluxes used in the slope simulations from 16 July 2020 to 15 July 2021. (**a**) Daily rainfall at Whiteknights. The maximum was 43.8 mm on 2 October 2020. (**b**) Daily reference potential evapotranspiration (PET) and the prescribed potential fluxes. Potential soil evaporation was 60% of PET for the unplanted control (C). For alfalfa alone (A) and alfalfa with the mycorrhiza-containing formulation (A + MF), PET was partitioned into 20% potential soil evaporation and 80% potential transpiration. Background shading indicates the seasons.

Rainfall and potential evaporation per horizontal area were projected onto the sloping surface. Admission was capped at $0.95k_s$ per slope-surface area. An unsaturated atmospheric face received admitted rainfall minus actual evaporation. If the flux solution implied positive pressure at the face, it switched to $h = 0$ and the hydraulic gradient determined its flux. The face returned to a flux condition whenever maintaining h = 0 would require more water than the available supply. This release criterion prevents a saturated boundary from supplying fictitious water. Infiltration was checked against rainfall supply at every accepted state; surface excess and exfiltration were included consistently in the water balance. Potential soil evaporation was 0.60PET for C and 0.20PET for planted treatments; potential transpiration was zero for C and 0.80PET for A and A + MF. These fractions were assumed, not measured crop coefficients. Actual soil evaporation was calculated by multiplying potential soil evaporation by a suction-dependent reduction factor. This factor equalled one at surface-layer suction heads $\leq$1 m of water and zero at $\geq$150 m, decreasing linearly with the logarithm of the suction head between these thresholds.

The initial water table was 2.0 m vertically below ground and subsequently evolved without a fixed groundwater head. Upslope inflow was based on the initial slope-parallel

Darcy throughflow. A constant drainage adjustment of 484.369 mm yr^{-1} for SC or 502.175 mm yr^{-1} for SS, referenced to the model window's horizontal plan area, was converted to discharge per unit width and subtracted uniformly over the initially saturated part of the upslope boundary. The resulting inflow was held constant in time; downslope discharge followed a head–responsive unit-gradient Darcy condition. The same soil-specific drainage adjustment was used across treatments, while reference throughflow depended on treatment-specific hydraulic conductivity. Each treatment's prescribed inflow was retained during sensitivity runs.

2.5.3. Root Water Uptake and Root-Zone Shear Strength

Root-water-uptake-combined potential transpiration, $T_p(t)$, a Feddes-type pressure-head response, $\alpha_F(h)$, and a normalised exponential root distribution [43]:

$$S_r(z,h,t) = T_p(t)\,\alpha_F(h)\,\beta_r(z), \tag{8a}$$

$$\beta_r(z) = \begin{cases} \frac{\exp(-z/\lambda_r)}{\lambda_r[1-\exp(-z_r/\lambda_r)]}, & 0 \le z \le z_r, \\ 0, & z > z_r, \end{cases} \qquad z_r = 0.50\ \text{m}, \quad \lambda_r = 0.10\ \text{m}. \tag{8b}$$

The stress response increased linearly from zero at h = −0.10 m to unity at h = −0.25 m, remained unity to h = −15 m, and declined linearly to zero at h = −80 m. A and A + MF shared these thresholds, λ_r = 0.10 m, z_r = 0.50 m and potential transpiration of 0.80PET. Whole-column root dry mass cannot determine an uptake-depth profile or canopy-scale water demand without root-area, leaf-area or transpiration measurements [44]. The common prescription therefore provides a controlled comparison of the measured k_s differences; it does not represent the hydraulic consequences of the measured A–A + MF biomass differences. Realised uptake may nevertheless differ because α_F depends on the simulated pressure head. Seasonal root growth, senescence and treatment-specific water-use demand were not simulated.

Depth-dependent apparent cohesion, $c_a(z)$, was fitted to the positive measurements at six depths by ordinary least squares on $\ln[c_a]$; c_a = 0 was assigned to both controls. Measured mobilised friction angles were linearly interpolated between sampling depths and held at the nearest measured value between the surface and 0.05 m and between 0.48 and 0.50 m. With pore air pressure as the gauge reference, the available shear resistance on a slope-parallel plane was calculated by the extended Mohr–Coulomb failure criterion [45], considering positive pore water pressures (saturated) and negative pore water pressure (matric suction):

$$\tau_f = c_a(z) + \max[\sigma_n - \max(u_w,0),0]\tan\phi_m(z) + \max(-u_w,0)\tan\phi_{b,\text{eff}}, \tag{9}$$

Here, $c_a(z)$ is the mobilised apparent-cohesion intercept (kPa), σ_n is total normal stress, and u_w is gauge pore water pressure. The dimensionless $\tan[\phi_m(z)]$ is the slope of the saturated terminal direct-shear envelope at $\delta h/L_0$ = 12.5%; it converts effective normal stress to frictional resistance. The mobilised angle ϕ_m was interpolated from Table 1 and is not an established peak or critical-state angle. Positive u_w reduces effective normal stress, clipped at zero. Negative u_w contributes suction resistance through $(-u_w)\tan\phi_{b,\text{eff}(z,t)}$. The main formulation uses effective saturation from the same retention relationship employed in seepage:

$$\tan\phi_{b,eff}(z,t) = S_e(z,t)\tan\phi_m(z) \tag{10}$$

Effective saturation, $S_e(z,t)$, was evaluated from the local simulated pressure head and the corresponding van Genuchten parameters at every state. Equation (10) follows the normalised-water-content weighting in the second prediction approach of Vanapalli

et al. [46], applied here to the measured mobilised composite angle, $\phi_m(z)$. The term $\tan\phi_{b,eff}$ is an effective secant coefficient for suction resistance, not the tangent slope of a nonlinear strength–suction envelope. Unsaturated shear tests were not performed, so this relation is a constitutive prediction rather than a measured or calibrated strength function.

2.5.4. Infinite-Slope Stability and Daily Critical Depth

At each scheduled state, pressure head was converted to $u_w = 9.81\ h$ kPa and interpolated at Z = {0.05, 0.06, . . ., 0.49 m}. The local calculation took the minimum over these depths. Candidate planes were parallel to the ground; circular, compound and toe-defined mechanisms were excluded.

For a potential plane at vertical depth, z, and time, t, the infinite-slope factor of safety was calculated as

$$F(z,t) = \frac{\tau_f(z,t)}{\gamma z\ \sin\beta\ \cos\beta} \tag{11}$$

The total normal stress on a slope-parallel plane at the vertical depth, z, was calculated as $\sigma_n = \gamma z \cos^2\beta$.

$$F_{RZ}(d) = \min_{j\in\{4,5\}} \min_{t\in T_d} \min_{z\in Z} F_j(z,t)\ Z = \{0.05, 0.06, \ldots, 0.49\ \text{m}\} \tag{12}$$

Here, τ_f is the resistance from Equation (9), γ is the assigned bulk unit weight and z is vertical depth, j identifies the two central hydraulic grid columns, T_d contains the four scheduled 6 h states for day (d), $F_j(z,t)$ is the factor of safety evaluated in column j using Equation (11), and F_{RZ} is the root-zone minimum factor of safety.

For each climatic day, d, the reported root-zone factor of safety was the minimum over the two central hydraulic grid columns (columns 4 and 5), all candidate depths and the four scheduled 6 h hydraulic states.

2.5.5. Numerical Verification

The numerical implementation was checked using a slope-parallel constant-total-head field. The maximum absolute interior Darcy-flux components were 1.2×10^{-25} and 5.5×10^{-25} m s^{-1} in the slope-parallel and slope-normal directions, respectively, indicating negligible numerical error. All transient calculations met the prescribed solver residual and water-balance criteria. The 2190 daily FoS results, representing 365 days for six cases, were finite and positive. The automated depth checks also confirmed that all critical slip planes were located between 0.05 and 0.49 m below the ground surface. The simulated mean groundwater-table depth varied between approximately 1.27 and 2.42 m, demonstrating a climate-driven response from the initial 2.0 m depth without imposing a fixed groundwater head. These checks confirm the numerical consistency of the local seepage and infinite-slope model. However, they do not validate the adopted constitutive relationships or assess deeper and global failure mechanisms.

2.5.6. Sensitivity Analyses

Retention sensitivity was assessed separately for C, A and A + MF in both soils. The parameter α was multiplied by 0.75 or 1.25 and n by 0.90 or 1.10, one at a time, with $m = 1 - 1/n$, giving 24 annual cases. These bounds were exploratory assumptions rather than measured treatment ranges. The parameters θ_r and θ_s, k_s, the measured c_a and ϕ_m profiles, initial pressure head and prescribed upslope inflow remained unchanged. Storage, relative conductivity and effective saturation in Equation (10) were recalculated using the perturbed retention function. Uptake sensitivity was assessed for A and A + MF only: λ_r was set to 0.05 or 0.20 m, retaining normalisation, or potential transpiration was set to 0.60 or 1.00 PET with evaporation adjusted to 0.40 or 0 PET. These 16 cases preserved total

potential demand. All 40 hydraulic perturbations covered the complete 365-day sequence. The treatment-specific annual minima are reported in Section 3.5.

Strength sensitivity re-evaluated every scheduled baseline hydraulic state with c_a multiplied by 0.5 or zero, then with both zero c_a and control friction, without recalculating seepage. The substituted friction angle was used consistently in both normal-stress friction and Equation (10). A further comparison set suction resistance to zero. These are comparisons with the uncapped baseline, not the measured confidence limits. For mechanism separation, the A and A + MF mechanical profiles were evaluated against both planted hydraulic histories in each soil and re-minimised over all depths, sections and times. Annual minima from different combinations can occur at different states; their differences are conditional contrasts, not additive mechanical and hydraulic percentages.

Storm sensitivity was analysed during 1–7 October 2020 for all six cases and 26 January–3 February 2021 for SS-A from their saved baseline antecedent states. Within each window, unchanged daily rainfall totals were applied over 24, 6 or 3 h starting at midnight, with hourly hydraulic reporting. The 24 h hourly run provided a matched temporal-resolution reference. All 21 event replays were completed. For each soil–treatment combination and rainfall duration, the lowest available event minimum was retained. The SC values and SS-C/SS-A + MF values are governed by October; SS-A is governed by January. Only SS-A was additionally replayed in January, so the summary does not compare all treatments under a common storm. These are event-window minima, not annual minima under an alternative year-round hyetograph. The six baselines and all 40 hydraulic perturbations were rerun with the same solver criteria. Independent re-minimisation of all 67 saved pressure histories reproduced the reported minima; the largest absolute cumulative water-balance residual was below 0.0082 mm.

3. Results

3.1. Plant Biomass and Saturated Hydraulic Conductivity

After five months, mean shoot dry mass was 2.673 and 2.937 g for SC-A and SC-A + MF, and 2.390 and 2.607 g for SS-A and SS-A + MF (Figure 6a), representing increases of 9.9% and 9.1%. The factorial model detected neither a soil effect ($p = 0.118$), treatment effect ($p = 0.208$), nor soil × treatment interaction ($p = 0.897$; Table 4). None of the six Tukey-adjusted comparisons among the four shoot-mass means was significant (all $p \geq 0.201$).

Mean recovered root dry mass was 0.0798 and 0.0993 g in SC and 0.0527 and 0.0807 g in SS for A and A + MF, respectively (Figure 6b). Soil and treatment effects were significant ($p = 0.00025$ and 0.00019), but the interaction was not ($F(1,8) = 1.31$, $p = 0.286$; Table 4). Across all four soil–treatment means, Tukey testing found A + MF greater than A in both SC ($p = 0.0233$) and SS ($p = 0.00297$). SC exceeded SS within both A ($p = 0.00364$) and A + MF ($p = 0.0295$), whereas SC-A and SS-A + MF did not differ ($p = 0.998$). The 24.5% and 53.2% increases are descriptive percentage contrasts and do not establish a stronger formulation response in SS.

The root-to-shoot index was R/S, where R and S are treatment mean root and shoot dry masses. It increased from 0.0298 to 0.0338 in SC and from 0.0220 to 0.0309 in SS. These values are ratios of treatment means, not means of paired individual-column ratios; no replicate-level standard error or significance test is assigned to them. The larger proportional change in SS was mainly below ground, although the absolute mean root dry mass remained greater in SC. Root diameter, architecture, area ratio, tensile strength and microbial colonisation were not measured, so biomass was not used directly as a reinforcement or water-uptake parameter.

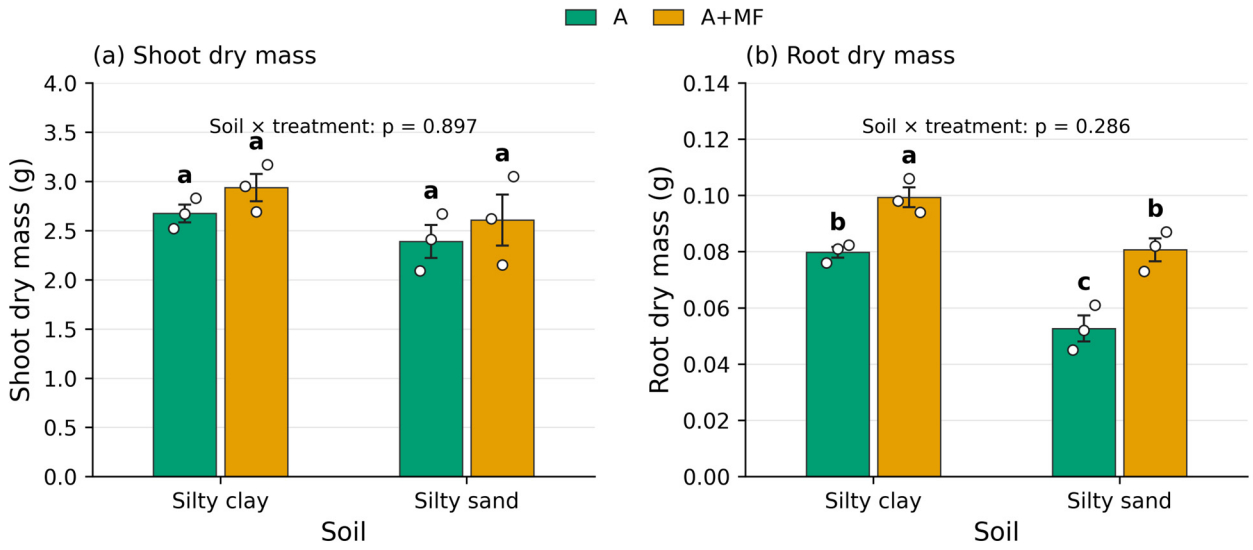


Figure 6. Alfalfa biomass after five months: (**a**) shoot dry mass and (**b**) recovered root dry mass. Bars show means, open circles individual columns, and error bars standard errors (n = 3 per soil–treatment combination). Within each panel, groups without a shared lower-case letter differ significantly according to Tukey's multiple-comparison test ($p < 0.05$). Letters in different panels are unrelated.

Table 4. Two-way ANOVA of shoot dry mass, recovered root dry mass and saturated hydraulic conductivity on their original measurement scales.

Response	Effect	df	F	p	η_p^2
Shoot mass	Soil	1, 8	3.06	0.118	0.277
	Treatment	1, 8	1.87	0.208	0.190
	Soil × treatment	1, 8	0.018	0.897	0.002
Root mass	Soil	1, 8	38.54	0.000257	0.828
	Treatment	1, 8	41.63	0.000198	0.839
	Soil × treatment	1, 8	1.31	0.286	0.141
Conductivity	Soil	1, 12	228.46	3.56×10^{-9}	0.950
	Treatment	2, 12	138.67	5.09×10^{-9}	0.959
	Soil × treatment	2, 12	15.19	0.000516	0.717

Note: df gives the numerator and denominator degrees of freedom; F is the ANOVA test statistic; p is the p-value; and η_p^2 is partial eta squared, a measure of effect size.

Mean k_s increased from C to A to A + MF (Figure 7): 0.067, 0.189 and 0.277 m d^{-1} in SC, and 0.198, 0.418 and 0.616 m d^{-1} in SS. The original-scale factorial model detected soil and treatment effects (both $p < 0.000001$) and an interaction ($F(2,12) = 15.19$, $p = 0.0005$; Table 4). With Tukey adjustment across all six means, SC-C differed from SC-A and SC-A + MF ($p = 0.00654$ and 0.0000513), whereas SC-A and SC-A + MF did not differ ($p = 0.055$). All three within-SS pairs differed (all $p < 0.0001$). For each matched treatment, SS exceeded SC (all $p \leq 0.0037$). The mean A + MF-versus-A increases were 46.6% and 47.4%; planted means were 2.83–4.15 times their control in SC and 2.11–3.11 times in SS. Contrasts with C include the different nutrient-management regime.

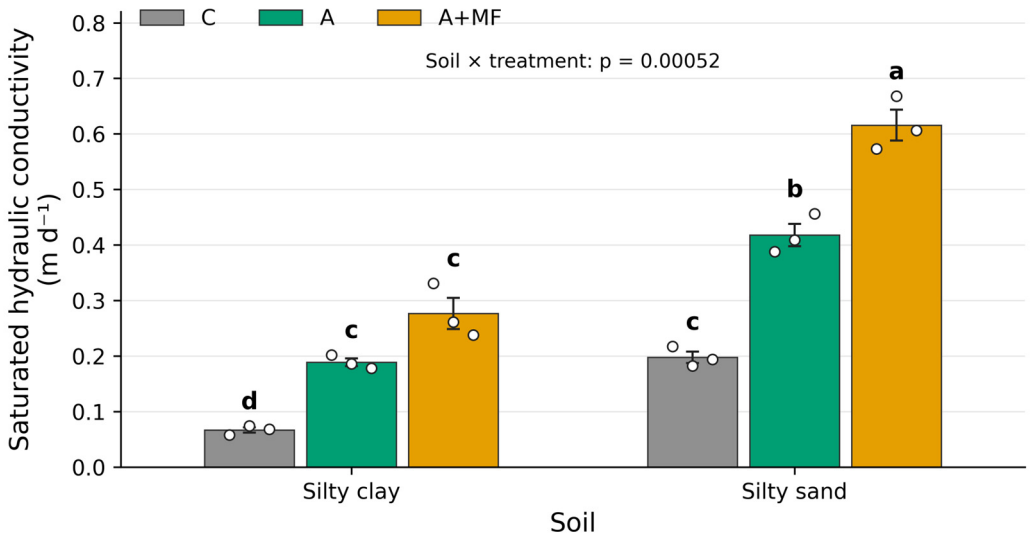


Figure 7. Saturated hydraulic conductivity of SC and SS under C, A and A + MF. Bars show means, open circles individual columns, and error bars standard errors (n = 3 per soil–treatment combination). Means without a shared lower-case letter differ at Tukey-adjusted $p < 0.05$ across all six soil–treatment groups following the original-scale two-way ANOVA (15 pairwise comparisons).

The interaction on the original scale indicates different absolute conductivity responses among these soil–treatment combinations. It was not significant after log transformation ($F(2,12) = 3.62$, $p = 0.0589$), so the data do not establish an interaction in proportional responses at the 5% threshold. This scale dependence and the small sample size qualify interpretation; neither a general texture effect nor equal proportional responses can be inferred. In the numerical analysis, A and A + MF shared the retention curves and potential water-use parameters within each soil. Their hydraulic differences therefore arose from the assigned k_s values rather than from prescribed differences in root distribution or atmospheric demand.

3.2. Saturated Mobilised Shear Response

The shear curves at 50 mm (Figure 8) and 90 mm (Figure 9) remained displacement hardening over the imposed range. At a common normal stress, planted specimens generally mobilised greater terminal shear resistance than C, with A + MF giving a further increment. Saturation removed matric suction as an explanation for these test contrasts. The response reflects treatment-associated changes in the saturated composite, but C–A and C–A + MF contrasts also include the nutrient-management difference and cannot be attributed exclusively to roots.

At 50 mm in SC, terminal stresses were approximately 13, 17 and 18 kPa for C, A and A + MF under 37 kPa normal stress, and approximately 35, 43 and 45 kPa under 100 kPa. Corresponding SS values were approximately 17, 19 and 20 kPa at 37 kPa, and 48, 51 and 52 kPa at 100 kPa. The SS control had the larger baseline resistance, whereas the absolute planted-treatment increments were generally larger in SC. At 90 mm, A + MF remained above A at the terminal displacement in both soils, although intermediate portions of the SS curves crossed. A single treatment ranking consequently does not describe every stage of shear mobilisation.

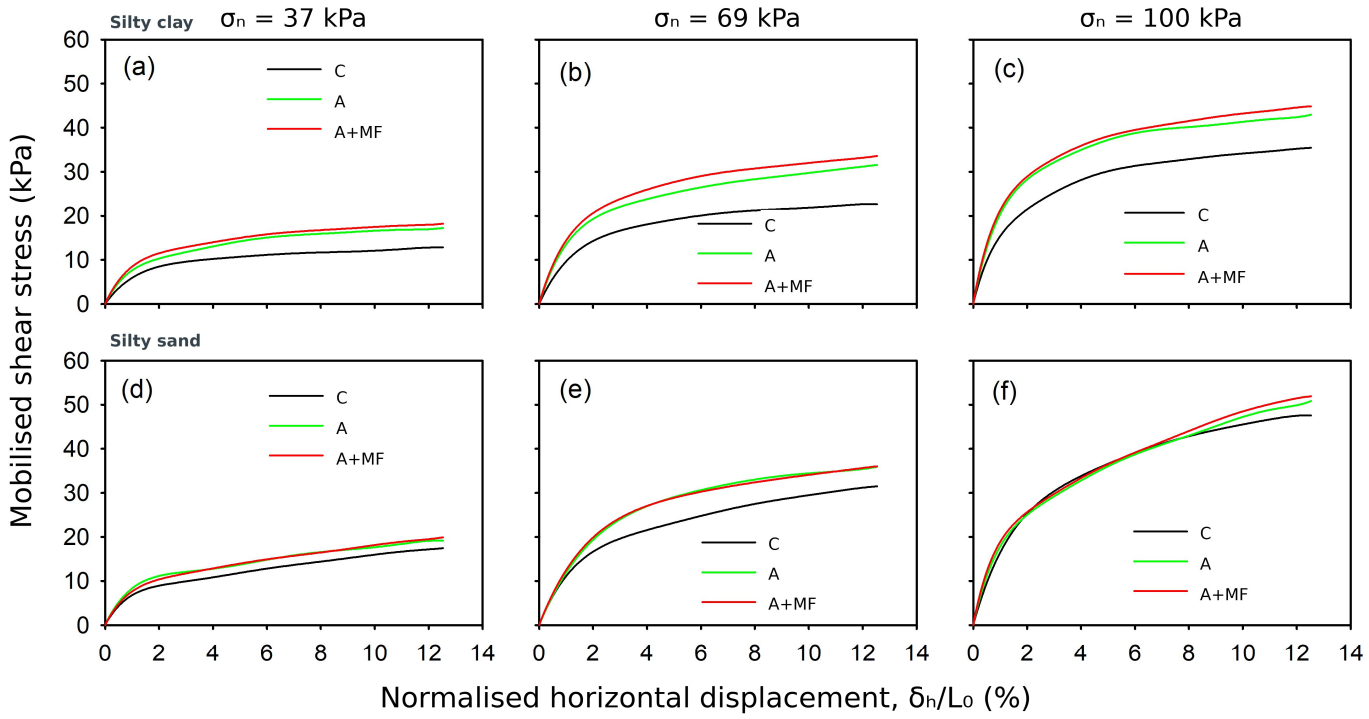


Figure 8. Saturated direct-shear response at 0.05 m depth. (**a**) SC at 37 kPa. (**b**) SC at 69 kPa. (**c**) SC at 100 kPa. (**d**) SS at 37 kPa. (**e**) SS at 69 kPa. (**f**) SS at 100 kPa. The stresses listed are applied normal stresses. The horizontal axis is normalised horizontal displacement, $100\delta h/L_0$ (%), with L_0 = 60 mm; it is not true shear strain. Terminal displacement is 7.5 mm, corresponding to 12.5%. C, unplanted control; A, alfalfa; A + MF, alfalfa with the formulation. No distinct peak was reached.

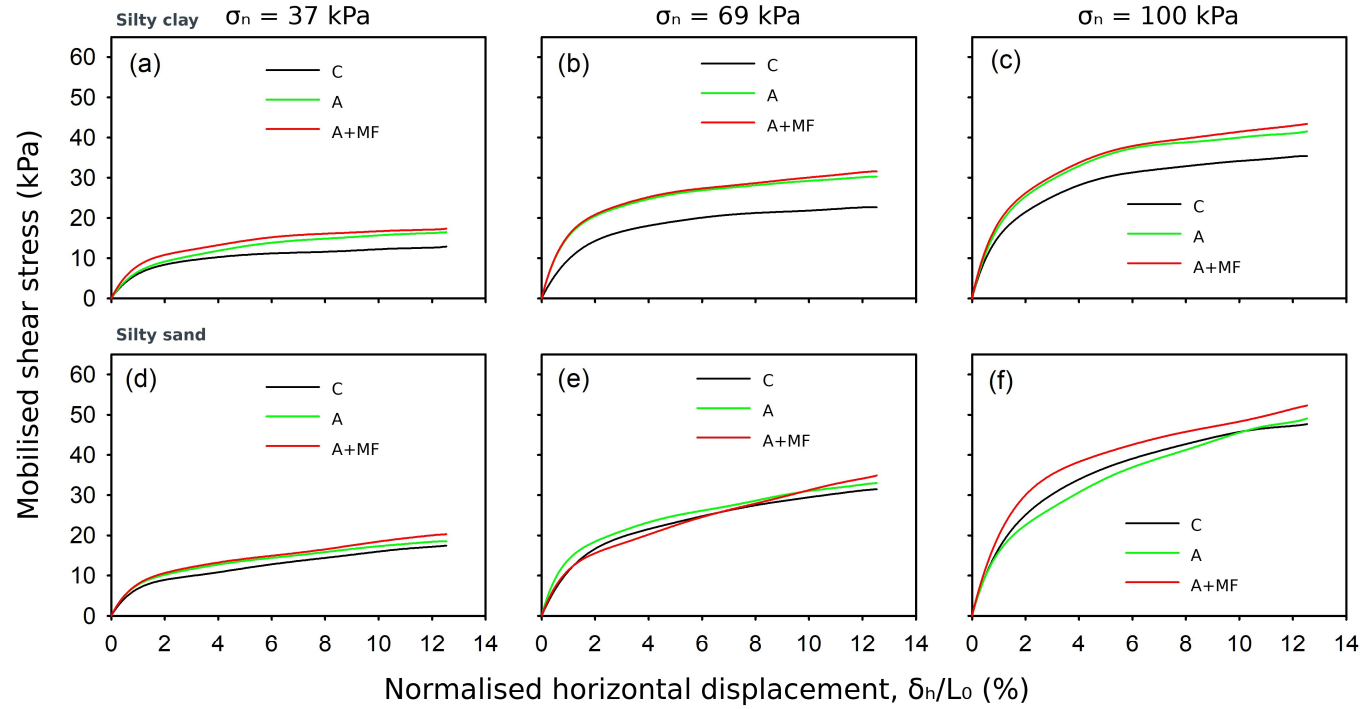


Figure 9. Saturated direct-shear response at 0.09 m depth. (**a**) SC at 37 kPa. (**b**) SC at 69 kPa. (**c**) SC at 100 kPa. (**d**) SS at 37 kPa. (**e**) SS at 69 kPa. (**f**) SS at 100 kPa. The stresses listed are applied normal stresses. Treatments and the normalised horizontal-displacement ratio are defined in Figure 8.

3.3. Reinforcement Magnitude and Depth Persistence

Apparent cohesion decreased with depth in all planted treatments (Table 1; Figure 10a,b). At 0.05 m, c_a was 3.76 and 4.71 kPa for SC-A and SC-A + MF, compared with 0.75 and 1.55 kPa for SS-A and SS-A + MF. At 0.30 m, the values were 0.75 and 1.05 kPa in SC and 0.015 and 0.45 kPa in SS. At 0.48 m, the SC values remained 0.30 and 0.40 kPa, while SS-A was zero and SS-A + MF retained 0.23 kPa. SC developed greater absolute apparent cohesion, whereas the formulation extended persistence more strongly relative to the rapidly decaying SS-A profile.

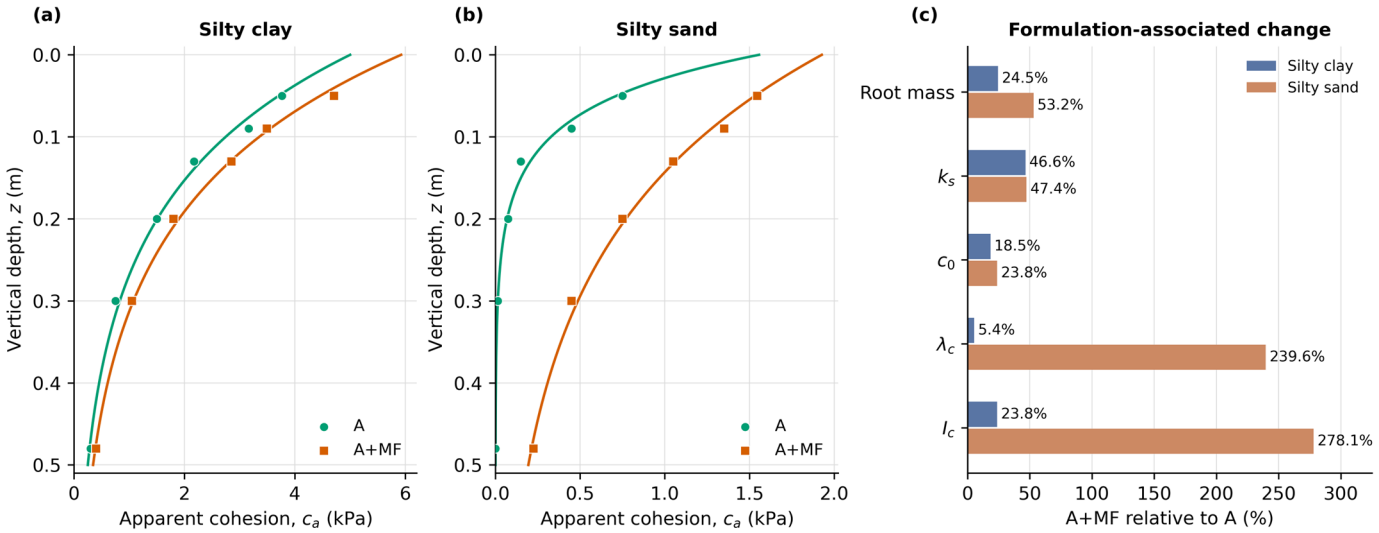


Figure 10. Depth-dependent treatment response. (**a**) Apparent-cohesion measurements from Table 1 and exponential fits for SC. (**b**) Apparent-cohesion measurements from Table 1 and exponential fits for SS. (**c**) Percentage changes in mean recovered root mass, mean saturated conductivity (*k*s), extrapolated cohesion c_0, decay depth λ_c and integrated apparent cohesion I_c over 0–0.50 m for A + MF relative to A. The zero SS-A point at 0.48 m is shown but excluded from logarithmic fitting. These are whole-formulation changes and do not isolate fungal causation.

Log-linear fitting of the positive values in Table 1 gave R^2 = 0.99 for SC-A/SC-A + MF and 0.98/0.99 for SS-A/SS-A + MF. In SC, c_0 increased from 5.0 to 5.93 kPa (+18.5%) and λ_c from 0.167 to 0.176 m (+5.4%). In SS, c_0 increased from 1.56 to 1.93 kPa (+23.8%), while λ_c increased from 0.064 to 0.218 m (+239.6%). The high R^2 values describe six positive depth values, or five for SS-A; they do not quantify uncertainty in the underlying three-point strength envelopes.

Integration over 0–0.50 m gave I_c = 0.79/0.98 kPa·m in SC and 0.10/0.38 kPa·m in SS for A/A + MF. The formulation-associated increases were 23.8% and 278.1%, calculated before rounding. SC retained the larger absolute index, whereas SS had the greater proportional increment. Assigned friction angles differed by typically 1–3° between treatments and describe the mobilised envelopes rather than an established change in intrinsic mineral friction.

3.4. Annual Root-Zone Stability

Root-zone FoS varied with climatic forcing under the SWRC-based strength relation (Figure 11). The annual minima for C/A/A + MF were 1.11/1.86/2.00 for SC and 1.78/2.43/2.38 for SS. All planted cases exceeded their controls. Five cases were governed on 3 October; SS-A was governed on 30 January.

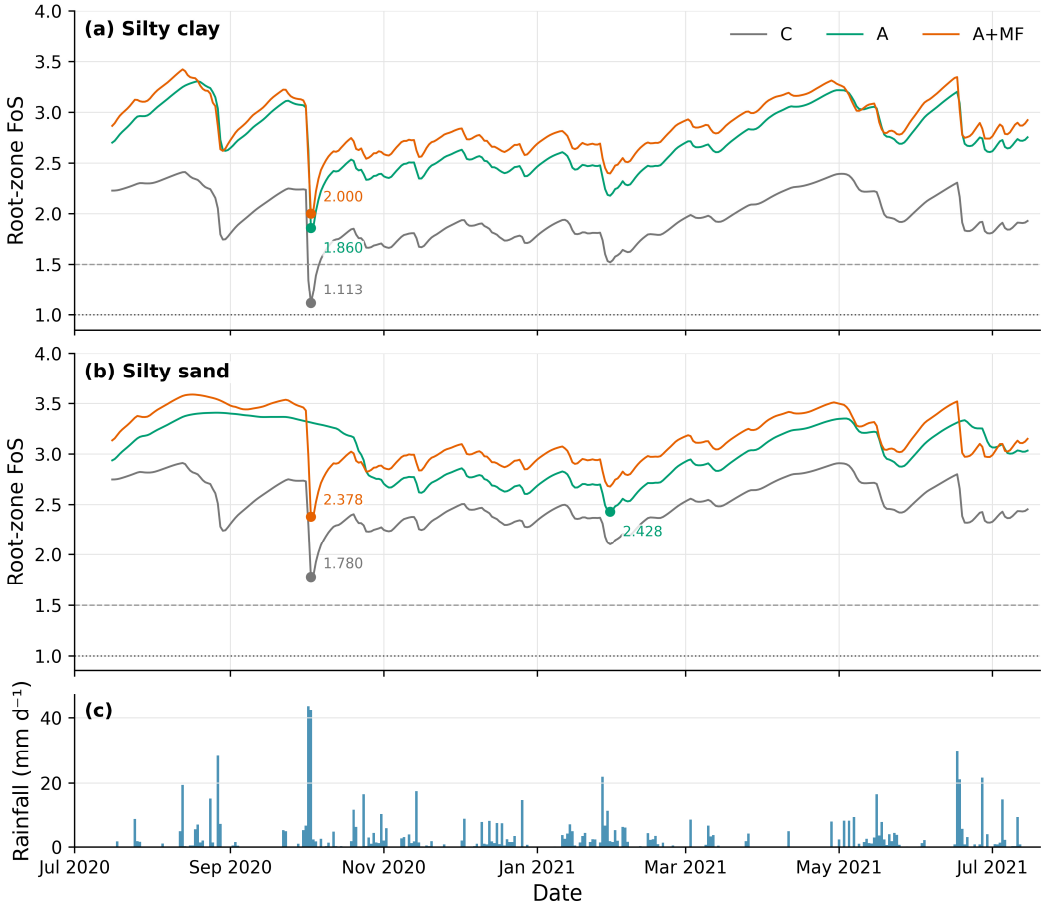


Figure 11. Daily minimum root-zone FoS from Equation (10). (**a**) Silty clay. (**b**) Silty sand. (**c**) Daily rainfall. FoS was minimised over 0.05–0.49 m depth. Symbols and labels mark annual minima. Lines at FoS = 1.0 and 1.5 are visual references.

The SC control approached FoS = 1.0 during October, while both planted SC cases and all SS cases remained above the 1.5 visual reference. These lines aid comparison and do not constitute site-specific design acceptance criteria.

Seasonal recovery followed the wet-period troughs. A + MF generally exceeded A in SC, while the planted SS curves crossed. The SS-A + MF annual minimum was 2.1% below SS-A despite stronger mechanical reinforcement. This coupled comparison depends on the pressure state, effective saturation and the strength profile.

3.5. Sensitivity and Matched-Input Comparisons

The retention perturbations affected all three treatments (Figure 12a,b). Annual minima ranged from 1.04–1.32, 1.52–2.25 and 1.70–2.17 for SC-C, SC-A and SC-A + MF, respectively; corresponding SS ranges were 1.55–1.92, 1.97–2.74 and 2.12–2.65. Both planted treatments retained higher minima than their corresponding control under each matched retention perturbation. The planted ordering nevertheless changed in some cases. In SC, multiplying n by 1.10 gave A/A + MF minima of 2.25/2.17, reversing the baseline A + MF > A ordering. In SS, multiplying α by 0.75 gave 2.22/2.46 and multiplying n by 0.90 gave 1.97/2.12, reversing the baseline A > A + MF ordering. These comparisons apply the same parameter perturbation to both treatments, rather than comparing a perturbed treatment with an unchanged baseline.

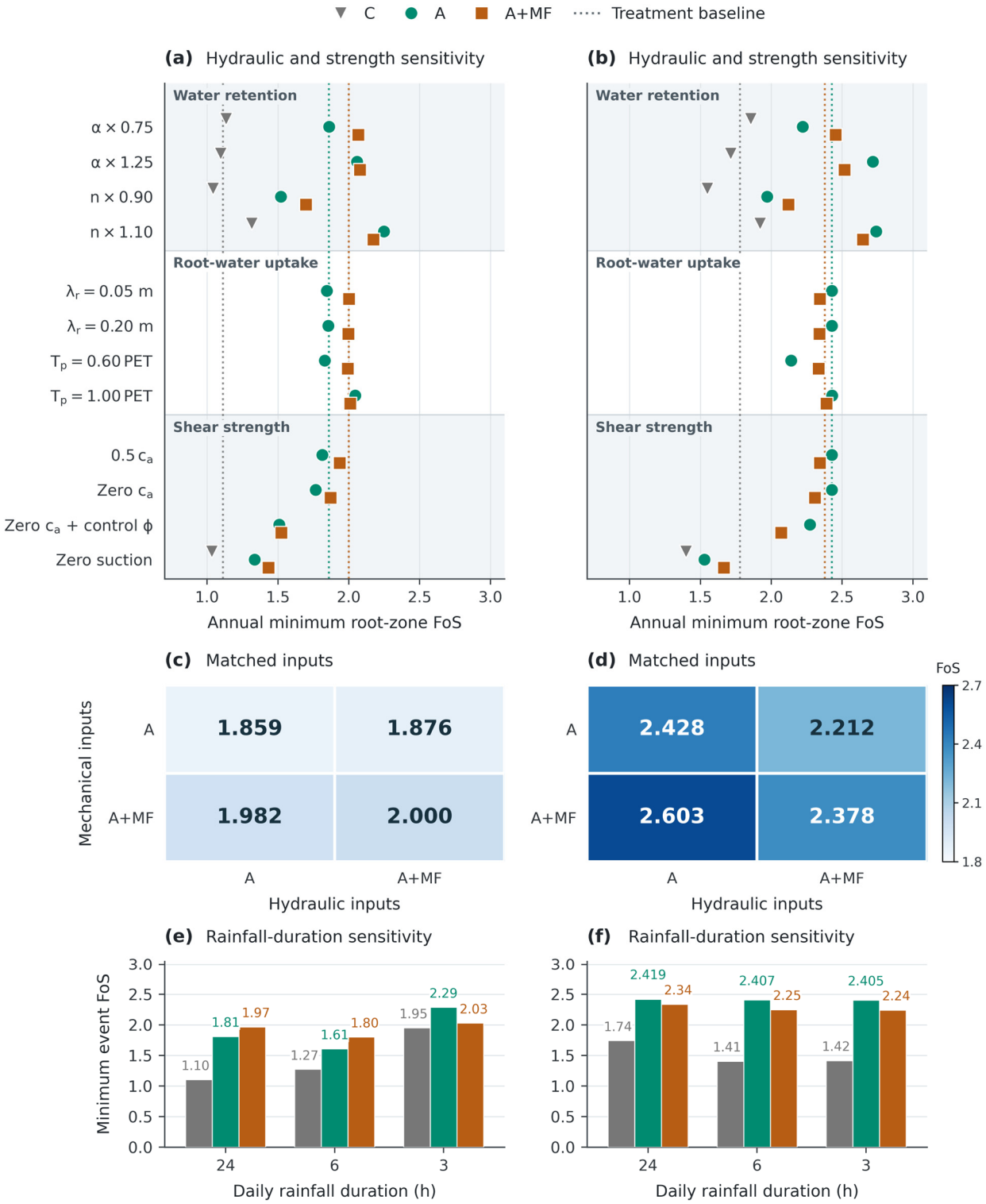


Figure 12. Sensitivity of minimum root-zone FoS in SC and SS. (**a**) Retention, uptake and strength perturbations for SC. (**b**) The same perturbations for SS. Dotted lines mark the treatment baselines. (**c**) Matched hydraulic and mechanical inputs for SC. (**d**) Matched inputs for SS. Rows identify mechanical inputs and columns identify hydraulic inputs. Panels (**c**,**d**) share a FoS colour scale. (**e**) Minimum event FoS by rainfall duration for SC. (**f**) Minimum event FoS by rainfall duration for SS. Grey, green and orange identify C, A and A + MF in (**a**,**b**,**e**,**f**).

Across the uptake perturbations, annual minima ranged from 1.83 to 2.05 for SC-A and from 1.99 to 2.01 for SC-A + MF; the SS ranges were 2.14–2.43 and 2.34–2.39, respectively (Figure 12a,b). Potential transpiration of 1.00 PET gave SC-A/A + MF minima of

2.05/2.01, whereas 0.60 PET gave SS-A/A + MF minima of 2.14/2.34. Both cases reversed the corresponding baseline planted ordering. The results quantify dependence on the prescribed uptake assumptions; the selected ranges are not measured treatment uncertainties or confidence intervals.

Reducing the fitted apparent-cohesion intercept changed the planted annual minima as follows (A/A + MF): SC: baseline 1.86/2.00, half c_a 1.81/1.94, zero c_a 1.77/1.87; SS: baseline 2.43/2.38, half c_a 2.43/2.34, zero c_a 2.43/2.31. The zero-cohesion cases are model perturbations rather than measured lower-confidence bounds. Figure 12a,b also shows the control-friction and zero-suction comparisons.

The matched-input annual minima were, for SC: A hydraulics with A/A + MF mechanics 1.86/1.98, and A + MF hydraulics with A/A + MF mechanics 1.88/2.00; for SS: A hydraulics with A/A + MF mechanics 2.43/2.60, and A + MF hydraulics with A/A + MF mechanics 2.21/2.38 (Figure 12c,d). Replacing A mechanics with A + MF mechanics increased resistance at a common hydraulic history and effective-saturation state. The hydraulic substitution could offset that mechanical gain, explaining the SS ordering within the model. Each combination was independently re-minimised.

The minimum event FoS varied with rainfall duration (Figure 12e,f). For durations of 24, 6 and 3 h, respectively, the SC minima were 1.10, 1.27 and 1.95 for C; 1.81, 1.61 and 2.29 for A; and 1.97, 1.80 and 2.03 for A + MF. Shortening the duration from 24 to 6 h reduced both planted SC minima, whereas further concentration into 3 h increased them. A + MF exceeded A under the 24 and 6 h scenarios, but A exceeded A + MF under 3 h rainfall. For SS, the lowest available event minima were 1.74, 1.41 and 1.42 for C; 2.42, 2.41 and 2.41 for A; and 2.34, 2.25 and 2.24 for A + MF. The SS-A reduction from 24 to 3 h was approximately 0.6%. These SS values summarise the available windows: C and A + MF are governed by October, whereas A is governed by January. They do not establish the three-treatment ordering under one common event, because January replays were completed only for SS-A.

4. Discussion

4.1. Biological and Hydraulic Responses in the Two Soils

The formulation increased mean recovered root dry mass by 24.5% in SC and 53.2% in SS. The A + MF–A contrasts were significant after Tukey adjustment across the four soil–treatment means. However, the root-mass interaction between soil and treatment was not significant ($p = 0.286$), so the larger percentage increase in SS does not establish a different formulation response between soils. No significant shoot-mass differences or soil × treatment interaction were detected. Root mass also gives only part of the mechanical picture: the resistance mobilised across a shear surface depends on root diameter, orientation, tensile behaviour, anchorage and contact with the soil [7,21].

These responses must be attributed to the commercial formulation. Although studies with verified fungal establishment have shown improvements in alfalfa performance and changes in rooted-soil hydrology [30,31], the product used here also contained Trichoderma, Bacillus, humic substances and seaweed-derived constituents. Without colonisation measurements, an inoculant-only treatment or a matched carrier control, the individual contributions of these components cannot be separated. A and A + MF shared the same planting, irrigation and nutrient regime, providing a common basis for assessing the added formulation. Comparisons with C also include nutrient management, because planted columns received low-phosphorus nutrient solution while controls received water.

Conductivity increased under the planted treatments, and SS was more conductive than SC within every matched treatment. A + MF exceeded A by 46.6% in SC and 47.4% in SS, although the globally adjusted comparison was significant only in SS. The signifi-

cant interaction on the original scale concerns differences in absolute conductivity. The interaction was not significant after log transformation, leaving the evidence for different proportional responses between soils inconclusive. Similar percentage increases therefore provide no basis for adopting a common hydraulic multiplier. Changes in pore connectivity and rhizosphere structure can affect rainfall entry, redistribution and drainage, linking mechanical reinforcement to changes in pore water pressure [15,16]. Previous work also shows that biological effects on permeability and retention depend on the soil and its compaction state [13,47–50].

4.2. Influence of Soil Texture on Root Reinforcement Profiles

Saturated direct-shear testing provided a common hydraulic reference for comparing mechanical resistance. Saturation removed matric suction as an explanation for the higher terminal shear resistance of A and A + MF. The measured differences therefore describe the mobilised response of each soil–treatment composite under the test conditions. This reference is useful because plant–soil reinforcement can vary with water regime [51], and the measurements at six depths showed that resistance also varied substantially within the root zone.

The fitted profiles revealed different patterns in the two soils. In SC, A + MF mainly increased reinforcement near the surface: c_0 rose from 5.002 to 5.926 kPa, while λc changed from 0.167 to 0.176 m. The integrated cohesion index, I_c, increased by 23.8%. In SS, the reinforcement amplitude was smaller, but λ_c increased from 0.064 to 0.218 m and Ic by 278.1%. SC thus retained the larger absolute reinforcement profile, while the main formulation response in SS was the persistence of reinforcement with depth.

The fitted parameters describe different aspects of this behaviour. The intercept c_0 is the extrapolated surface amplitude, and λ_c is the depth at which the exponential profile falls to about 37% of that value. Together, they determine the apparent cohesion, $c_a(z)$, available at a potential slip plane. The index I_c is the area under the profile over a stated depth and allows comparisons over a common root-zone thickness. It has units of kPa·m and cannot be used directly as cohesion in a stability calculation. Profiles with the same I_c can still provide different resistance at a particular depth. Representing the root zone by one constant cohesion would lose this information [20], whereas depth-specific profiles recognise the influence of root distribution and orientation on slope reliability [9,52].

The strength envelopes remain uncertain, particularly at the low stresses relevant to shallow failures. Each envelope used one specimen at each of three normal stresses between 37 and 100 kPa, so stress effects and specimen variability could not be separated. The available data did not support reliable confidence intervals. At a normal stress of 5 kPa and zero suction, the fitted 0.05 m envelopes predict shear resistances of approximately 5.79 and 6.83 kPa for SC-A and SC-A + MF, and 3.19 and 4.09 kPa for SS-A and SS-A + MF. Setting ca to zero reduces these values to 2.02 and 2.12 kPa in SC and 2.44 and 2.55 kPa in SS. The reduced- and zero-cohesion cases in Figure 12a,b show how this extrapolation affects the annual minimum FoS; replicated tests at lower stresses are needed to assess it experimentally.

4.3. Coupled Hydrology and Seasonal Stability

Under the SWRC-based strength relation, annual minimum FoS increased from 1.11 in SC-C to 1.86 in SC-A and 2.00 in SC-A + MF. The corresponding SS values were 1.78, 2.43 and 2.38. Both planted treatments exceeded their controls, but adding the formulation increased the minimum in SC and slightly reduced it in SS. The SS result shows how less favourable hydraulic conditions can offset additional mechanical resistance, even where reinforcement persists to greater depths.

All three SC cases, SS-C and SS-A + MF reached their annual minima on 3 October, following 86.4 mm of rainfall over 2–3 October. SS-A reached its minimum on 30 January after the late-January wet period. FoS recovered as rainfall decreased and the soil dried, consistent with the time-dependent contribution of hydraulic reinforcement [11,12]. Higher conductivity can promote both wetting and drainage, so its effect on stability depends on the pressure history and boundary forcing.

The matched-input comparisons clarify this balance (Figure 12c,d). With the hydraulic history held constant, the A + MF mechanical properties increased the minimum FoS in both soils. Substituting the A + MF hydraulic history could offset that benefit through stronger wetting or reduced suction. Each combination was therefore searched again for its controlling date and depth. Since these conditions can change, separate annual minima cannot be used to assign additive percentage contributions to mechanical and hydraulic reinforcement.

The retention and uptake sensitivities also changed the treatment rankings (Figure 12a,b). The baseline planted ordering reversed in SC when n was multiplied by 1.10, and in SS when α was multiplied by 0.75 or n by 0.90. Selected uptake assumptions produced further reversals. Retention affects both the calculated pressure history and the effective-saturation weighting of suction resistance. The shared baseline retention curve and uptake prescription therefore simplify processes that require treatment-specific measurements.

4.4. Interpretation and Limits of Root-Zone Factor of Safety

The calculated FoS describes stability within the experimentally characterised root zone. All four planted cases reached their baseline minima at 0.49 m, the deepest plane considered, compared with 0.31 m for SC-C and 0.48 m for SS-C. Repeated selection of the lower search boundary makes the depth restriction particularly important [53]. The search covered 0.05–0.49 m and excluded deeper translational failures, circular or compound mechanisms, and effects associated with finite crest or toe geometry. A high value within this shallow zone therefore cannot establish the stability of the complete slope.

Rainfall timing introduces a further limitation. The annual baseline spread each daily total uniformly over 24 h and recorded results every 6 h. The hourly event replays retained the antecedent conditions and daily rainfall totals within each window while applying rain over 24, 6 or 3 h (Figure 12e,f). The SC October treatment ordering reversed between the 24 and 3 h cases, whereas the January minimum for SS-A changed by approximately 0.6%. The SS panel combines the lowest available minima from October for C and A + MF and January for A. Its unequal window coverage prevents interpretation as a treatment comparison under one common storm.

The higher SC minima under 3 h rainfall coincided with less water entering the soil and more runoff under the imposed infiltration cap. This response depends on that boundary assumption and does not imply that more intense rainfall generally improves stability. The constructed rainfall patterns also omit measured storm timing and sub-hourly peaks. These event results describe the selected replay windows rather than the response to a full year of concentrated rainfall.

Several biological and hydraulic assumptions also need validation. A single growth state after five months was retained throughout the meteorological year, without seasonal rooting, senescence or canopy change. Uptake sensitivities used λ_r values of 0.05 and 0.20 m and potential transpiration of 0.60 and 1.00 PET. They assess the chosen uptake assumptions, without establishing how the measured biomass differences affect water demand. Treatment-specific ks was also assigned throughout the 4 m hydraulic window, although it was measured in 0.5 m columns. The transfer of these measurements to depth, the lateral drainage assumptions and field heterogeneity remain sources of uncertainty [54].

The retention perturbations did not examine changes in θs or θr, hysteresis, preferential flow or retention that changes with time. In addition, the SWRC-based suction-strength relation has not been validated by unsaturated shear tests on these rooted composites [46]. The zero-suction cases in Figure 12a,b quantify the model's dependence on that assumed resistance.

4.5. Implications for Shallow Slope Assessment

Treatment selection should consider the resistance available at the likely slip depth together with the soil's response to rainfall and drying. Reporting c_0, λ_c and the full $c_a(z)$ profile, alongside the sampling depths and mobilisation criterion, would allow mechanical results to be transferred more consistently into stability calculations. Hydraulic characterisation should include conductivity, retention and plant water use. The present results support comparisons within the two investigated soils and modelling conditions; broader relationships with soil texture and values for field design require further evidence.

The most useful next steps are replicated low-stress shear tests, measurements of root architecture and fungal colonisation, and retention and transpiration measurements for each treatment. Field pore-water-pressure monitoring and sub-daily rainfall records would help assess the simulated hydraulic response. Where deeper failure or crest and toe geometry matters, the approach also needs comparison with finite-slope analyses that allow a wider range of failure surfaces, including established Bishop and Spencer methods [55,56]. Combining these measurements with depth-resolved reinforcement would strengthen the use of column experiments for assessing shallow slope performance under climatic loading.

5. Conclusions

The column experiment and slope calculations support the following conclusions, with measured and model-dependent findings distinguished.

1. A + MF increased mean recovered root dry mass by 24.5% in SC and 53.2% in SS relative to alfalfa alone. Both differences were significant using Tukey's multiple-comparison test, while shoot-mass differences were not significant. The soil × treatment interaction for biomass was also not significant, so the larger percentage increase in SS does not establish a stronger formulation response in that soil. These findings describe the commercial formulation as a whole; planted–control comparisons also include differences in nutrient management.
2. Mean saturated conductivity increased by 46.6% in SC and 47.4% in SS under A + MF relative to A. Using Tukey's test across all six soil–treatment groups, the A + MF–A difference was significant in SS but not in SC. Compared with the unplanted control, A + MF significantly increased conductivity in both soils. The soil × treatment interaction was significant for absolute conductivity but not after log transformation, indicating that the evidence for different proportional responses between soils remains inconclusive.
3. Mechanical reinforcement varied with depth. The fitted decay depths, λ_c, were 0.167 and 0.176 m in SC and 0.064 and 0.218 m in SS for A and A + MF, respectively. The corresponding integrated cohesion indices over 0–0.50 m were approximately 0.79 and 0.98 kPa·m in SC, and 0.10 and 0.38 kPa·m in SS. SC retained the greater absolute reinforcement, whereas SS showed the larger proportional increase in persistence. I_c allows comparisons between profiles, while stability calculations require the local $c_a(z)$. Extrapolation from the tested normal stresses of 37–100 kPa to shallow field stresses remains uncertain.
4. Under the adopted SWRC-based strength relation, annual minimum FoS values for C, A and A + MF were 1.11, 1.86 and 2.00 in SC, and 1.78, 2.43 and 2.38 in SS. October wetting governed five cases, while SS-A reached its minimum in late January.

Matched-input comparisons showed that the A + MF mechanical properties increased the minimum FoS when pressure history and effective saturation were held constant. Changes in hydraulic conditions could offset this benefit, explaining why stronger reinforcement did not always produce a higher annual minimum.

5. Some retention, root-water-uptake and rainfall-duration sensitivity scenarios reversed the A versus A + MF ranking. The reduced-cohesion and suction-strength comparisons further demonstrated the influence of the modelling assumptions. These scenarios are exploratory comparisons, not statistical confidence intervals. The results apply to the two investigated soils and the prescribed 0.05–0.49 m root-zone search, which excludes deeper and global failure mechanisms. Treatment-specific water-retention measurements, replicated low-stress and unsaturated shear tests, and field validation are needed before quantitative design use.

Author Contributions: Conceptualization, M.N.; methodology, A.R. and M.N.; investigation, A.R.; formal analysis, A.R. and M.N.; data curation, A.R.; writing—original draft preparation, A.R.; writing—review and editing, M.N.; funding acquisition, M.N. All authors have read and agreed to the published version of the manuscript.

Funding: This research was supported by the University of West London Vice-Chancellor's PhD Scholarship awarded to A.R.; no external grant number applies.

Institutional Review Board Statement: Not applicable.

Informed Consent Statement: Not applicable.

Data Availability Statement: The data supporting the findings of this study are available from the corresponding author upon reasonable request.

Conflicts of Interest: The authors declare no conflicts of interest.

References

1. Li, C.; Cheng, Q.; Tang, C.; Gu, Y.; Cui, L.; Guo, H. Effects of layer thickness on desiccation cracking behaviour of a vegetated soil. *Biogeotechnics* **2024**, *2*, 100068. [CrossRef]
2. Löbmann, M.T.; Geitner, C.; Wellstein, C.; Zerbe, S. The influence of herbaceous vegetation on slope stability—A review. *Earth-Sci. Rev.* **2020**, *209*, 103328. [CrossRef]
3. Bischetti, G.B.; De Cesare, G.; Mickovski, S.B.; Rauch, H.P.; Schwarz, M.; Stangl, R. Design and temporal issues in soil bioengineering structures for the stabilisation of shallow soil movements. *Ecol. Eng.* **2021**, *169*, 106309. [CrossRef]
4. Ng, C.W.W.; Zhang, Q.; Zhou, C.; Ni, J. Eco-geotechnics for human sustainability. *Sci. China Technol. Sci.* **2022**, *65*, 2809–2845. [CrossRef]
5. Preti, F.; Capobianco, V.; Sangalli, P. Soil and Water Bioengineering (SWB) is and has always been a nature-based solution (NBS): A reasoned comparison of terms and definitions. *Ecol. Eng.* **2022**, *181*, 106687. [CrossRef]
6. Bordoni, M.; Cislaghi, A.; Vercesi, A.; Bischetti, G.B.; Meisina, C. Effects of plant roots on soil shear strength and shallow landslide proneness in an area of northern Italian Apennines. *Bull. Eng. Geol. Environ.* **2020**, *79*, 3361–3381. [CrossRef]
7. Li, Y.; Zhou, M.; Zuo, H.; Wang, Q.; Xing, Y.; Yan, G. Root traits and mechanical properties of three shrubland species: Implications for bioengineered slope stability. *Environ. Eng. Sci.* **2021**, *38*, 1176–1187. [CrossRef]
8. Liu, Y.-F.; Meng, L.-C.; Huang, Z.; Shi, Z.-H.; Wu, G.-L. Contribution of fine roots mechanical property of Poaceae grasses to soil erosion resistance on the Loess Plateau. *Geoderma* **2022**, *426*, 116122. [CrossRef]
9. Masi, E.B.; Segoni, S.; Tofani, V. Root reinforcement in slope stability models: A review. *Geosciences* **2021**, *11*, 212. [CrossRef]
10. Capobianco, V.; Robinson, K.; Kalsnes, B.; Ekeheien, C.; Høydal, Ø. Hydro-mechanical effects of several riparian vegetation combinations on the streambank stability: A benchmark case in southeastern Norway. *Sustainability* **2021**, *13*, 4046. [CrossRef]
11. Feng, S.; Liu, H.W.; Ng, C.W.W. Analytical analysis of the mechanical and hydrological effects of vegetation on shallow slope stability. *Comput. Geotech.* **2020**, *118*, 103335. [CrossRef]
12. Ni, J.J.; Leung, A.K.; Ng, C.W.W.; Shao, W. Modelling hydro-mechanical reinforcements of plants to slope stability. *Comput. Geotech.* **2018**, *95*, 99–109. [CrossRef]
13. Pauwels, R.; Graefe, J.; Bitterlich, M. An arbuscular mycorrhizal fungus alters soil-water retention and hydraulic conductivity in a soil-texture-specific way. *Mycorrhiza* **2023**, *33*, 165–179. [CrossRef] [PubMed]

14. Yildiz, A.; Graf, F.; Rickli, C.; Springman, S.M. Assessment of plant-induced suction and its effects on the shear strength of rooted soils. *Proc. Inst. Civ. Eng. Geotech. Eng.* **2019**, *172*, 507–519. [CrossRef]
15. Leung, A.K.; Garg, A.; Coo, J.L.; Ng, C.W.W.; Hau, B.C.H. Effects of the roots of *Cynodon dactylon* and *Schefflera heptaphylla* on water infiltration rate and soil hydraulic conductivity. *Hydrol. Process.* **2015**, *29*, 3342–3354. [CrossRef]
16. Ni, J.J.; Leung, A.K.; Ng, C.W.W. Modelling effects of root growth and decay on soil water retention and permeability. *Can. Geotech. J.* **2019**, *56*, 1049–1055. [CrossRef]
17. Cecconi, M.; Tagarelli, V.; Cotecchia, F.; Pane, V.; Anselmucci, F.; Bertolini, I.; Biondi, G.; Boldrin, D.; Capobianco, V.; Cardile, G.; et al. Soil-Vegetation-Atmosphere Interaction for Engineering Applications: Recent Multi-Scale and Multi-Disciplinary Insights. *Geomech. Energy Environ.* **2025**, *43*, 100723. [CrossRef]
18. Badakhshan, E.; Vaunat, J. Thermo-Hydro-Mechanical Modeling of Root–Soil Interaction in Unsaturated Slopes. *Comput. Geotech.* **2026**, *192*, 107931. [CrossRef]
19. Park, J.; Kim, I.; Kang, J.-K. Root reinforcement effect on cover slopes of solid-waste landfill in soil bioengineering. *Sustainability* **2021**, *13*, 3991. [CrossRef]
20. Nguyen, T.S.; Likitlersuang, S.; Jotisankasa, A. Influence of the spatial variability of the root cohesion on a slope-scale stability model: A case study of residual soil slope in Thailand. *Bull. Eng. Geol. Environ.* **2019**, *78*, 3337–3351. [CrossRef]
21. Schwarz, M.; Giadrossich, F.; Cohen, D. Modeling root reinforcement using a root-failure Weibull survival function. *Hydrol. Earth Syst. Sci.* **2013**, *17*, 4367–4377. [CrossRef]
22. Waldron, L.J.; Dakessian, S.; Nemson, J.A. Shear resistance enhancement of 1.22 mdiameter soil cross sections by pine and alfalfa roots. *Soil Sci. Soc. Am. J.* **1983**, *47*, 9–14. [CrossRef]
23. Zhou, X.; Wei, Y.; Li, D.; Jiang, J.; Zhang, C. Strengthening effects of alfalfa roots on soil shear resistance in loess region. *Sci. Soil Water Conserv.* **2019**, *17*, 53–59. [CrossRef]
24. Xing, S.; Zhang, G.; Zhu, P.; Wang, L.; Wang, Z.; Wang, C. Variation in shear strength of soil–root systems under five typical land-use types on the Loess Plateau of China. *Catena* **2023**, *222*, 106883. [CrossRef]
25. Johnson, N.C. Resource stoichiometry elucidates the structure and function of arbuscular mycorrhizas across scales. *New Phytol.* **2010**, *185*, 631–647. [CrossRef] [PubMed]
26. Koide, R.T.; Mosse, B. A history of research on arbuscular mycorrhiza. *Mycorrhiza* **2004**, *14*, 145–163. [CrossRef] [PubMed]
27. Kakouridis, A.; Hagen, J.A.; Kan, M.P.; Mambelli, S.; Feldman, L.J.; Herman, D.J.; Weber, P.K.; Pett-Ridge, J.; Firestone, M.K. Routes to roots: Direct evidence of water transport by arbuscular mycorrhizal fungi to host plants. *New Phytol.* **2022**, *236*, 210–221. [CrossRef] [PubMed]
28. Bast, A.; Wilcke, W.; Graf, F.; Lüscher, P.; Gärtner, H. Does mycorrhizal inoculation improve plant survival, aggregate stability, and fine root development on a coarse-grained soil in an alpine eco-engineering field experiment? *J. Geophys. Res. Biogeosci.* **2016**, *121*, 2158–2171. [CrossRef]
29. Graf, F.; Frei, M. Soil aggregate stability related to soil density, root length, and mycorrhiza using site-specific *Alnus incana* and *Melanogaster variegatus* s.l. *Ecol. Eng.* **2013**, *57*, 314–323. [CrossRef]
30. Pellegrino, E.; Nuti, M.; Ercoli, L. Multiple arbuscular mycorrhizal fungal consortia enhance yield and fatty acids of *Medicago sativa*: A two-year field study on agronomic traits and tracing of fungal persistence. *Front. Plant Sci.* **2022**, *13*, 814401. [CrossRef] [PubMed]
31. Roberts-Self, E.G.; Tarantino, A. Arbuscular mycorrhizal fungi effect on the hydrological regime in vegetated soil. *Géotechnique* **2026**, *76*, 973–985. [CrossRef]
32. *BS 1377-1:2016*; Methods of Test for Soils for Civil Engineering Purposes—General Requirements and Sample Preparation. BSI: London, UK, 2016.
33. *BS 1377-2:2022*; Methods of Test for Soils for Civil Engineering Purposes—Classification Tests and Determination of Geotechnical Properties. BSI: London, UK, 2022.
34. *BS 1377-4:1990*; Methods of Test for Soils for Civil Engineering Purposes—Compaction-Related Tests. BSI: London, UK, 1990.
35. Chandler, R.J.; Crilly, M.S.; Montgomery-Smith, G. A low-cost method of assessing clay desiccation for low-rise buildings. *Proc. Inst. Civ. Eng. Civ. Eng.* **1992**, *92*, 82–89. [CrossRef]
36. *BS 1377-5:1990*; Methods of Test for Soils for Civil Engineering Purposes—Compressibility, Permeability and Durability Tests. BSI: London, UK, 1990.
37. Richards, L.A. Capillary conduction of liquids through porous mediums. *Physics* **1931**, *1*, 318–333. [CrossRef]
38. van Genuchten, M.T. A closed-form equation for predicting the hydraulic conductivity of unsaturated soils. *Soil Sci. Soc. Am. J.* **1980**, *44*, 892–898. [CrossRef]
39. Mualem, Y. A new model for predicting the hydraulic conductivity of unsaturated porous media. *Water Resour. Res.* **1976**, *12*, 513–522. [CrossRef]

40. University of Reading. Atmospheric Observatory Data: Climatological Observations Data Extractor, Whiteknights, Reading. Available online: https://research.reading.ac.uk/meteorology/atmospheric-observatory/atmospheric-observatory-data/ (accessed on 7 August 2026).
41. Dalle Piagge, M.J.; Robinson, E.L.; Kay, A.L.; Chapman, R.; Bell, V.A.; Blackford, K.R.; Blyth, E.M. *Potential Evapotranspiration Derived from HadUK-Grid 1 km Gridded Climate Observations 1969–2024 (Hydro-PE HadUK-Grid)*; NERC EDS Environmental Information Data Centre: Lancaster, UK, 2026. [CrossRef]
42. Allen, R.G.; Pereira, L.S.; Raes, D.; Smith, M. *Crop Evapotranspiration: Guidelines for Computing Crop Water Requirements*; FAO Irrigation and Drainage Paper 56; Food and Agriculture Organization of the United Nations: Rome, Italy, 1998.
43. Feddes, R.A.; Kowalik, P.J.; Zaradny, H. *Simulation of Field Water Use and Crop Yield*; Pudoc: Wageningen, The Netherlands, 1978.
44. Ng, C.W.W.; Garg, A.; Leung, A.K.; Hau, B.C.H. Relationships between leaf and root area indices and soil suction induced during drying–wetting cycles. *Ecol. Eng.* **2016**, *91*, 113–118. [CrossRef]
45. Fredlund, D.G.; Morgenstern, N.R.; Widger, R.A. The shear strength of unsaturated soils. *Can. Geotech. J.* **1978**, *15*, 313–321. [CrossRef]
46. Vanapalli, S.K.; Fredlund, D.G.; Pufahl, D.E.; Clifton, A.W. Model for the prediction of shear strength with respect to soil suction. *Can. Geotech. J.* **1996**, *33*, 379–392. [CrossRef]
47. Leung, A.K.; Garg, A.; Ng, C.W.W. Effects of plant roots on soil-water retention and induced suction in vegetated soil. *Eng. Geol.* **2015**, *193*, 183–197. [CrossRef]
48. Pauwels, R.; Jansa, J.; Püschel, D.; Müller, A.; Graefe, J.; Kolb, S.; Bitterlich, M. Root growth and presence of *Rhizophagus irregularis* distinctly alter substrate hydraulic properties in a model system with *Medicago truncatula*. *Plant Soil* **2020**, *457*, 131–151. [CrossRef]
49. David, P.; Jana, R.; Radka, S.; Jan, J.; Michael, B. Soil compaction reversed the effect of arbuscular mycorrhizal fungi on soil hydraulic properties. *Mycorrhiza* **2024**, *34*, 361–368. [CrossRef] [PubMed]
50. Tagarelli, V.; Stasi, N.; Cotecchia, F.; Cafaro, F. Root-induced changes in the hydraulic properties of a fine slope cover. *E3S Web Conf.* **2024**, *544*, 16002. [CrossRef]
51. Gonzalez-Ollauri, A.; Mickovski, S.B. Plant–soil reinforcement response under different soil hydrological regimes. *Geoderma* **2017**, *285*, 141–150. [CrossRef]
52. Guo, H.; Qu, C.; Liu, L.; Zhang, Q.; Liu, Y. Reliability analysis of vegetated slope considering spatial variability of soil and root properties. *Comput. Geotech.* **2024**, *169*, 106257. [CrossRef]
53. Cheng, P.; Wu, L.; Zhang, H.; Zhou, J. Inclusion of root water absorption and reinforcement in upper bound limit stability analysis of vegetated slopes. *Comput. Geotech.* **2024**, *169*, 106227. [CrossRef]
54. Roberts-Self, E.G.; Tarantino, A. Experimental investigation and conceptual modelling of water-limited transpiration as hydraulic boundary condition in geotechnical engineering problems. *Géotechnique* **2026**, *76*, 1155–1169, 1–15. [CrossRef]
55. Bishop, A.W. The use of the slip circle in the stability analysis of slopes. *Géotechnique* **1955**, *5*, 7–17. [CrossRef]
56. Spencer, E. A method of analysis of the stability of embankments assuming parallel inter-slice forces. *Géotechnique* **1967**, *17*, 11–26. [CrossRef]

Disclaimer/Publisher's Note: The statements, opinions and data contained in all publications are solely those of the individual author(s) and contributor(s) and not of MDPI and/or the editor(s). MDPI and/or the editor(s) disclaim responsibility for any injury to people or property resulting from any ideas, methods, instructions or products referred to in the content.